Chapter 2

Investigation of Magnetic Anisotropy and SOD Activity of a Series of Pentagonal Bipyramidal Mn(II) Complexes

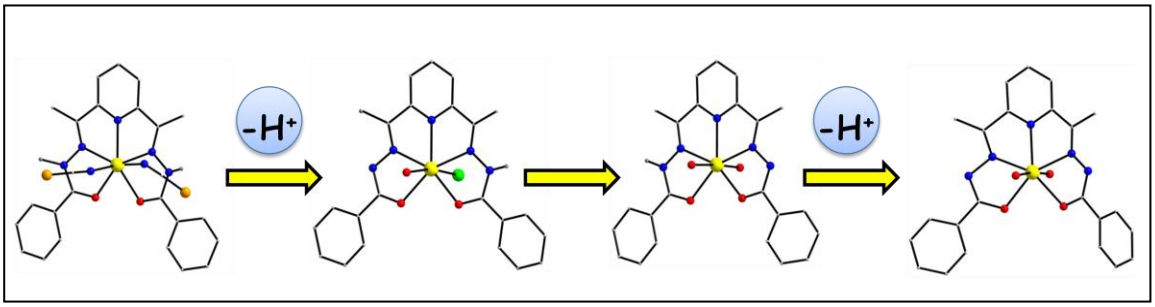

Abstract: Systematic studies of magnetic anisotropy in a series of pentagonal bipyramidal Mn(II) complexes have been carried out by using magnetization measurements and DFT calculations. Significantly large deviation in the axial zero field splitting parameters were observed on subtle modification of the coordination environment around the pentagonal bipyramidal Mn(II) center. Further, the influence of the coordination environment on the superoxide scavenging ability of these Mn(II) complexes were also evaluated.

2.1. Introduction

Mononuclear manganese (II) complexes are gaining considerable attention due to their implications in various scientific domains such as biochemistry and catalysis [1]. In biological systems, Mn(II) complexes are present in the active sites of several enzymes such as superoxide dismutase (SOD), catalase, ribonucleotide reductase, peroxidases, etc.[2-3]. The role of Mn(II) ion in the active sites of these enzymes are being subjected to extensive investigation due to their relevance in pharmacology [4]. Tremendous research efforts are currently being focused on developing model Mn(II) compounds which can effectively mimic these enzymes and thus develop abiotic catalyst for similar chemical transformations. This accounts for the recent surge in synthesis of Mn(II) complexes having coordination geometry/environment similar to those present in the active sites of the enzymes and subsequent investigation of their catalytic properties [5-9]. However, due to the lack of accurate structural data, the precise coordination geometry around the Mn(II) centres in the active sites of many enzymes have not been accurately deciphered so far. The lack of structural data is further aggravated by the fact that no useful information is generally obtained from electronic spectroscopic studies of Mn(II) complexes due to the spin forbidden nature of d-d-transitions in all coordination geometries.

In view of the above, experimental electronic structure determination of Mn(II) ions in active sites of different enzymes have traditionally relied on electron paramagnetic resonance (EPR) and subsequent structural correlation of the EPR data [10-11]. In these studies, the geometry and coordination environment around the Mn(II) centers were generally predicted with regard to the position and width of the EPR spectral lines. The advent of multifrequency high field/high frequency EPR has led to an outburst of activity in exploration of precise electronic structure in synthetic as well as biological Mn(II) complexes [12]. In this regard, structural correlations based on zero field splitting has emerged as a versatile probe in precise and unambiguous electronic structure determination of mononuclear Mn(II) complexes.

In all coordination geometry, high spin Mn(II) ion (d^5) has a singly degenerate ground electronic state, ^6S, electronic spin state S = 5/2 and nuclear spin state I = 5/2. The spin Hamiltonian ($\hat{H}$) of an orbitally degenerate high spin d^5 configuration is generally expressed by the equation-

$$\hat{H} = D[S_z^2 - \{S(S+1)\}/3] + E[S_x^2 - S_y^2] + g\beta HS + IAS,$$

where, the first two terms are the zero field splitting (ZFS) interactions with D and E representing the axial and the rhombic ZFS terms respectively. The third term is the Zeeman interaction term and the last term indicates the nuclear hyperfine interactions.

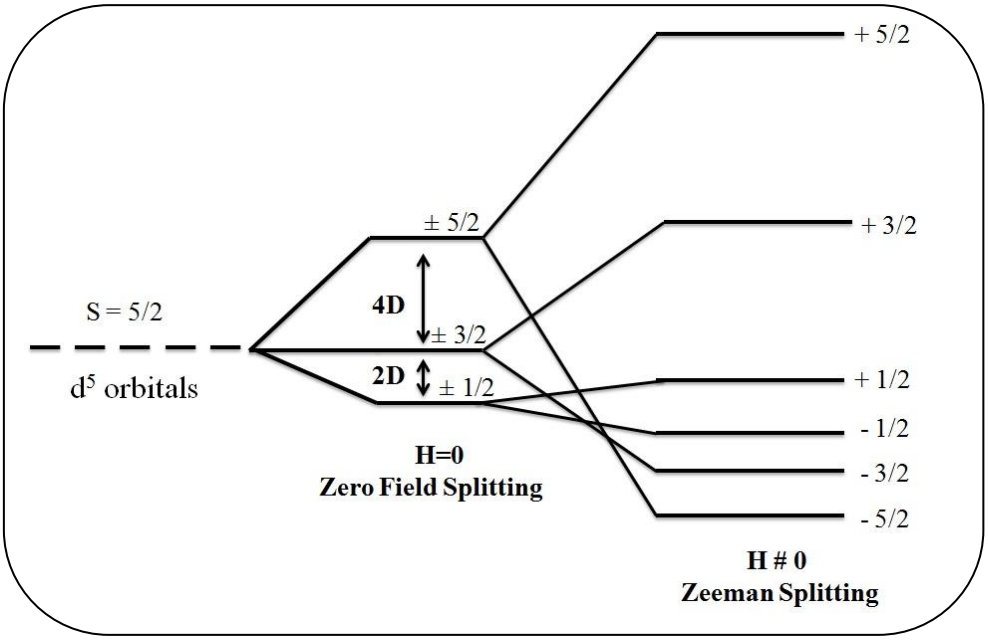

Figure 2.1. Schematic representation of Zero Field Splitting in d^5 systems

Due to the spherically symmetric electron density of the ^6S ground electronic state in high spin Mn(II), the in-state orbital angular momentum of the ground electronic state is negligible. Therefore, the anisotropy of the Zeeman interaction in Mn(II) ion is very small and the g values generally lie close to 2. Moreover, there exist only one possibility of distributing five spin up electrons in five d-orbitals and therefore no other sextet excited states are available for SOC of the ground ^6S state with excited electronic levels of identical spin multiplicity. Apart from that the metal-ligand bonds in Mn(II) complexes generally show very poor covalency and therefore the energy of the ligand to metal charge transfer states are too high for any meaningful SOC with the ground ^6S state (Figure 2.1). These eventually rules out the possibility of inducing out-of-state orbital angular momentum in the ground electronic state and therefore the magnitude of ZFS in Mn(II) complexes are expected to be rather small.

Recent works on accurate determination of ZFS in high spin mononuclear Mn(II) complexes show that the axial ZFS parameter, D generally lie between 0-1.21 cm^{-1} [13-22]. Moreover, systematic studies on a series of four, five and six-coordinate mononuclear Mn(II) dihalide complexes reveal that ZFS is not dependent on

coordination geometry of the complex and instead relies on the nature of halide ligands present. The observed trend of the magnitude of D is $D_I > D_{Br} > D_{Cl}$ and it is attributed to the ligand field strength of the halide ligands ($\Delta_I < \Delta_{Br} < \Delta_{Cl}$) [13-17]. However, recent studies have established that the mutual disposition of the two halide ligands also play a crucial role as ZFS of cis-dihalide Mn(II) complexes were found to be approximately two times less than the corresponding trans isomers [23].

In contrast to five- and six-coordinate Mn(II) complexes, very little investigations have been carried out to probe ZFS of seven-coordinated Mn(II) complexes. To the best of our knowledge, ZFS of only four seven-coordinated Mn(II) complexes have been reported so far and no concrete rationalization with regard to structure, geometry or coordination environment could be drawn so far (Chart 2.1) [24-26]. It is pertinent to note here that seven coordinate complexes Mn(II) complexes show efficient SOD activity comparable to native MnSOD and therefore the relevance of seven-coordinate Mn(II) in biological systems are being increasingly investigated [27-28].

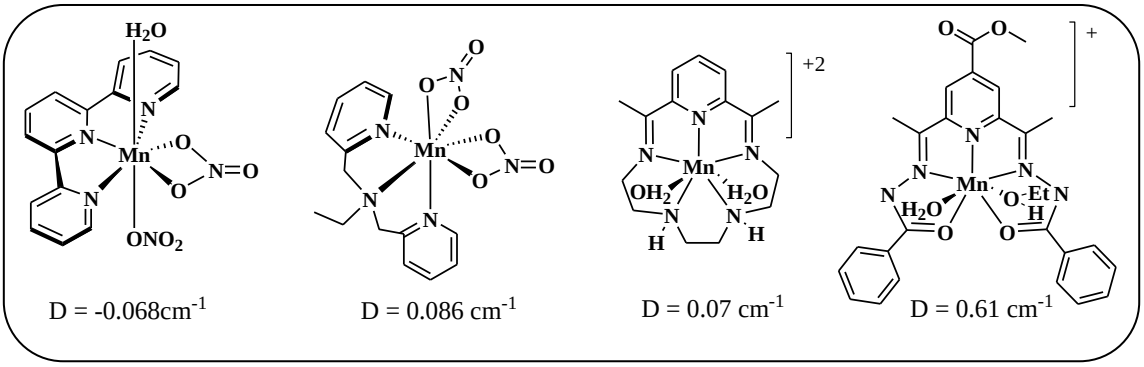

Chart 2.1. Examples of seven coordinate Mn(II) complexes for which D values have been determined

Moreover, several first row transition metal ions e.g. Fe^{2+}, Co^{2+} and Ni^{2+} show large axial ZFS parameter in seven-coordinate geometry and it is observed that the coordination environment plays a crucial role in determining the D parameter. Thus, a systematic study on ZFS of a series of pentagonal bipyramidal (PBP) Mn(II) complexes with subtle differences in their coordination environment was carried in this study.

The planar pentadentate ligand 2,6-diacetylpyridine bis(benzoyl hydrazone) (H_2L) is widely recognized for its ability to stabilize transition metal ions in PBP geometry (Chart 2.2). This acyclic ligand (H_2L) used in this work can be easily prepared by condensation of 2,6-diacetyl pyridine with phenyl hydrazine [29]. Due to the presence

of five ligating atoms in this planer acyclic molecule, it has been extensively used for assembling PBP complexes of a plethora of transition metal as well as lanthanide ions [30].

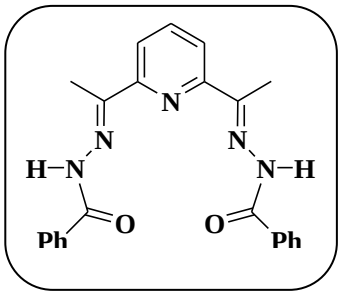

Chart 2.2.The ligand 2,6-diacetylpyridine bis(benzoyl hydrazone) (H_2L)

Herein, we have reported the synthesis, characterization, crystal structures and magnetic susceptibility measurements of four PBP Mn(II) complexes $[Mn(H_2L)(SCN)_2].4H_2O$ (**1**), $[Mn(HL)(H_2O)Cl].2H_2O$ (**2**), $[Mn(HL)(H_2O)_2]ClO_4$ (**3**), $[Mn(L)(H_2O)_2]$ (**4**). The ZFS of all four complexes were determined by magnetization measurements and DFT based theoretical calculations were performed to rationalize the experimental results. Moreover, superoxide dismutase activity of these complexes have been studied spectrophotometrically by using indirect nitro blue tetrazolium (NBT) assay.

2.2. Experimental Section

2.2.1. Materials and Methods

Starting materials were procured from commercial sources and used as received. Solvents were purified by conventional techniques and distilled prior to use. Elemental analyses were performed on a Perkin Elmer Model PR 2400 Series II Elemental Analyzer. Infrared spectra were recorded on a Nicolet Impact I-410 FT-IR spectrometer as KBr diluted discs and a Perkin Elmer MIR-FIR FT-IR spectrometer. The UV-visible spectra were recorded in a Shimadzu UV 2550 spectrophotometer. Melting points were recorded on a Buchi M-560 Melting Point apparatus and are reported uncorrected. Magnetic susceptibility data were collected on microcrystalline samples over a 2-300 K temperature range with an applied field of 1000 Oe using a MPMS SQUID magnetometer. Magnetization studies were performed between 0-5 T at 2 K, 5 K, 7 K and 10 K. 2, 6-diacetylpyridine bis(benzoyl hydrazone) i.e., H_2L and

$[Mn(H_2L)(H_2O)Cl]Cl$ were prepared according to the reported literature procedure [31-32].

2.2.2. Synthesis of $[Mn(H_2L)(SCN)_2].4H_2O$ (1)

To a solution of $[Mn(H_2L)(H_2O)Cl]Cl$ (0.015 mmol, 0.009 g) in 15 mL methanol, $K_2[Co(SCN)_4]$ (0.015 mmol, 0.0055 g) dissolved in 5 mL distilled water was added without agitation. The reaction mixture was kept undisturbed in dark for slow evaporation at room temperature. Orange block shaped crystals were observed after 10 days. The mother liquor was discarded and crystals were extracted separately, washed with ethanol and diethyl ether and air dried. Characterization data for (**1**): Yield: 0.0062 g (65% based on Mn). M. p. >250°C; Elemental analysis: Found C, 46.11%; H, 4.02%; N, 14.96%. $C_{25}H_{29}N_7O_6S_2Mn$ requires C, 46.74%; H, 4.55%; N, 14.96%. IR (KBr, cm^{-1}): 3420(br), 2106(m), 2094(s), 1624(m), 1577(m), 1537(w), 1490(s), 1447(w), 1381(m), 1290(s), 1159(w), 1075(s), 1028(w), 899(w), 809(s), 707(m), 625(w), 471(w).

2.2.3. Synthesis of $[Mn(HL)(H_2O)Cl].2H_2O$ (2)

To a solution of $[Mn(H_2L)(H_2O)Cl]Cl$ (0.03 mmol, 0.018 g) in 30 mL methanol and stirred for 10 minutes. Then, $K_3[Fe(CN)_6]$ (0.005 mmol, 0.0017 g) dissolved in 1 mL distilled water was added without agitation. The reaction mixture was kept undisturbed in dark for slow evaporation at room temperature. Orange block shaped crystals were observed after two weeks. The mother liquor was discarded and crystals were extracted separately, washed with ethanol and diethyl ether and air dried. Characterization data for (**2**): Yield: 0.0098 g (60% based on Mn); M. p. >250°C; Elemental analysis: Found C, 51.22%; H, 5.02%; N, 12.07%. $C_{23}H_{26}N_5O_5Mn$ requires C, 50.89%; H, 4.83%; N, 12.90%. IR (KBr, cm^{-1}): 3385(br), 1674(m), 1571(m), 1490(s), 1403(w), 1361(s), 1162(w), 1097(s), 1023(s), 867(w), 801(s), 713(m), 689(m), 427(w).

2.2.4. Synthesis of $[Mn(HL)(H_2O)_2]ClO_4$ (3)

To a solution of $[Mn(H_2L)(H_2O)Cl]Cl$ (0.1 mmol, 0.0602 g) in 5 mL methanol, $NaClO_4.H_2O$ (0.1 mmol, 0.0140 g) dissolved in 10 mL distilled water was added. Stirring was continued for two hours at room temperature. The reaction mixture was kept undisturbed for slow evaporation at room temperature. Orange needle shaped

crystals were observed after three weeks. The mother liquor was discarded and crystals were extracted separately, washed with ethanol and diethyl ether and air dried. Characterization data for (**3**): Yield: 0.1020 g (85 % based on Mn); M. p. >250°C; Elemental analysis: Found C, 45.78 %; H, 3.99%; N, 11.21%. $C_{46}H_{48}N_{10}O_{17}Mn_2Cl_2$ requires C, 46.29%; H, 4.05%; N, 11.73%. IR (KBr, cm^{-1}): 3464(br), 1698(w), 1620(s), 1532(m), 1486(s), 1366(s), 1297(s), 1089(s), 801(m), 709(s), 621(s), 520(m), 429(w).

2.2.5 Synthesis of $[Mn(L)(H_2O)_2]$ (4)

To a solution of $[Mn(H_2L)(H_2O)Cl]Cl$ (0.027 mmol, 0.016 g) in 15 mL methanol, NaN_3 (0.054 mmol, 0.0035 g) dissolved in 5 mL distilled water was added. Stirring was continued for three hours at room temperature. Then, the $K_3[Fe(CN)_6]$ (0.027 mmol, 0.008 g) dissolved in 10 mL distilled water was added without agitation. The reaction mixture was kept undisturbed for slow evaporation at room temperature. Dark brown block shaped crystals were observed after a week. The mother liquor was discarded and crystals were extracted separately, washed with ethanol and diethyl ether and air dried. Characterization data for (**4**): Yield: 0.0081 g (62 % based on Mn); M. p. >250°C; Elemental analysis: Found C, 55.92%; H, 4.80%; N, 14.23%. $C_{23}H_{23}N_5O_4Mn$ requires C, 56.57%; H, 4.75%; N, 14.34%. IR (KBr, cm^{-1}): 3435(br), 1643(m), 1585(s), 1494(s), 1407(w), 1359(s), 1160(s), 1044(m), 899(w), 705(w), 682(m).

2.2.6. Determination of SOD activity

The SOD activity of the Mn(II) complexes were measured by using a modified nitro blue tetrazolium (NBT) assay [33-34]. Reduction of NBT by alkaline DMSO, which acts as a source of superoxide radical ion ($O_2^{-\cdot}$) produces a blue formazan dye which can be easily detected spectrophotometrically. The % inhibition of NBT reduction was monitored against different concentration of the Mn(II) complexes. In general, 100 µL of 1.5 mM NBT was added to 1.5 mL of 0.2 M potassium phosphate buffer (pH 7.8). The tubes were kept in ice for 15 min. Then, 1.4 mL of alkaline DMSO solution was added with stirring. The absorbance was recorded at 630 nm against a sample prepared under similar condition except the addition of NaOH in DMSO. The compounds were added to the above condition before the addition of alkaline DMSO. Each experiment was performed in duplicate for different concentrations of the compounds. The

concentration required to produce 50% inhibition (IC_{50}) of the reduction of NBT has been determined by linear fitting of the curve.

2.2.7. Single Crystal X-Ray Diffraction Studies

Suitable single crystals of all the compounds obtained directly from the reaction mixtures were used for diffraction measurements. The diffraction data for the compounds were collected on a Bruker APEX-II CCD diffractometer using MoKα radiation (λ=0.71073 Å) using φ and ω scans of narrow (0.5°) frames at 90-100K. All the structures were solved by direct methods using SHELXL-97 as implemented in the WinGX program system [35]. Anisotropic refinement was executed on all non-hydrogen atoms. The aliphatic and aromatic hydrogen atoms were placed on calculated positions but were allowed to ride on their parent atoms during subsequent cycles of refinements. Positions of N-H and O-H hydrogen atoms were located on a difference Fourier map and allowed to ride on their parent atoms during subsequent cycles of refinements.

Continuous shape analysis was performed on the complexes using SHAPE program to determine the geometry of the Mn(II) compounds [36]. The data obtained from the analysis are listed in Table 2.1.

Table 2.1. Shape analysis data for compounds **1**-**4** using SHAPE program

Complex	**HP-7**	**HPY-7**	**PBPY-7**	**COC-7**	**CTPR-7**	**JPBPY-7**	**JETPY-7**
1	32.272	22.404	0.602	6.911	4.902	3.339	20.548
2	33.491	20.260	1.267	6.805	5.187	5.447	21.106
3	32.477	22.001	0.567	7.344	5.806	3.477	22.259
4	32.082	20.164	0.931	6.443	5.118	3.752	20.876

HP-7: Heptagon (D_{7h}); HPY-7:Hexagonal pyramid (C_{6v}); PBPY-7:Pentagonal bipyramid (D_{5h}); COC-7:Capped octahedron (C_{3v}); CTPR-7: Capped trigonal prism (C_{2v}); JPBPY-7: Johnson pentagonal bipyramid J13 (D_{5h}); JETPY-7: Johnson elongated triangular pyramid J7 (C_{3v}).

Table 2.2. Crystal data and refinement parameters of compounds **1-4**

Complex	**1**	**2**	**3**	**4**
Empirical formula	$C_{25}H_{21}N_7O_6S_2Mn$	$C_{23}H_{26}N_5O_5MnCl$	$C_{46}H_{48}N_{10}O_{17}Mn_2Cl_2$	$C_{23}H_{23}N_5O_4Mn$
Formula weight	636.52	542.88	1193.72	484.37
Temperature/K	296	100	100	296
Crystal system	Monoclinic	Triclinic	Triclinic	Monoclinic
Space group	*P2(1)/n*	*P-1*	*P-1*	*C2/c*
a/Å	11.446 (5)	8.983 (11)	9.816 (5)	11.617 (11)
b/Å	15.850 (7)	10.911 (13)	9.932 (5)	15.772 (15)
c/Å	16.456 (7)	13.553 (17)	14.941 (7)	7.425 (4)
α/°	90	95.89 (2)	71.70 (4)	90
β/°	98.19 (2)	100.07 (2)	89.25 (4)	94.02 (7)
γ/°	90	111.79 (2)	68.55 (4)	90
Volume/$Å^3$	2955.4 (2)	1194.00 (3)	1278.76 (12)	5926.5 (9)
Z	4	2	1	8
ρ_{calc}, g cm^{-3}	1.431	1.510	1.550	1.086
μ/mm^{-1}	0.772	0.710	0.681	0.476
Crystal size, mm^3	0.41x0.32x0.26	0.36x0.27x0.16	0.31x0.17x0.12	0.31x0.24x0.05
F(000)	1300	562	614	1992
Reflections collected	29091	4723	22652	29080
Data/parameters/restraints	7349/378/0	3813/346/0	6396/392/6	7325/300/0
Goodness-of-fit on F^2	1.043	1.036	0.990	0.807
Final R indexes [I>=2σ (I)]	R_1= 0.0510,wR_2=0.1415	R_1= 0.0383, R_2=0.0921	R_1= 0.0673,wR_2=0.1454	R_1= 0.765, wR_2=0.1967
Final R indexes [all data]	R_1= 0.0829, wR_2=0.1659	R_1= 0.0459, wR_2=0.0976	R_1= 0.1712, wR_2=0.1811	R_1= 0.2220 wR_2=0.2272

2.2.8. Theoretical Calculations

The theoretical calculations were performed with the ORCA program package [37]. All the calculations were carried out on the experimental crystal structures of compounds **1**-**4** using BP86 functional and the Karlsruhe polarized triple-zeta valence (TZVP) basis set [38-40]. The BP86 functional was found to be a reasonable choice for Mn(II) compounds than the more expensive hybrid functional [24]. Tight convergence criteria and denser integration grids (Grid 4) were also used for better accuracy. Spin unrestricted DFT together with the spin-orbit mean field (SOMF) representation of the SOC operator was used to calculate the EPR parameters of all mononuclear Mn(II) compounds [40]. Contribution of SOC to ZFS was calculated by considering four types of excitations as described by Neese and co-workers [42]. The $\alpha\rightarrow\alpha$ (SOMO$\rightarrow$VMO) and $\beta\rightarrow\beta$ (DOMO$\rightarrow$SOMO) excitations couple excited state of same multiplicity with the ground state. The $\alpha\rightarrow\beta$ (SOMO$\rightarrow$SOMO) and $\beta\rightarrow\alpha$ (DOMO$\rightarrow$VMO) excitations couple the ground state with excited states of multiplicity S-1 and S+1 respectively [25].

2.3. Results and Discussions

2.3.1. Synthesis and characterization of $[Mn(H_2L)(SCN)_2].4H_2O$ (1)

Recently, it has been reported that bridging thiocyanate ligand can induce substantial exchange interaction between spin carriers and this has spurred the development of several heterometallic thiocyanate based assemblies [44-46]. However, no thiocyanate bridged complex featuring seven coordinated metal ion has been so far reported and therefore we carried out the reaction of $[Mn(H_2L)Cl(H_2O)]Cl$ with $K_2[Co(SCN)_4]$ in aqueous methanol at room temperature (Scheme 2.1).

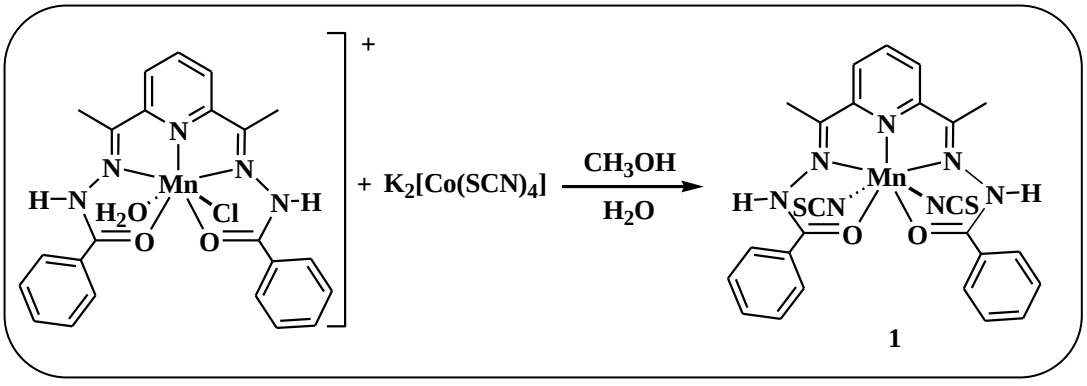

Scheme 2.1. Synthesis of compound **1**

It was anticipated that the thiocyanato ligand in $[Co(SCN)_4]^{2-}$ will replace the axial ligand in $[Mn(H_2L)Cl(H_2O)]Cl$ and thus result in heterometallic Mn(II)-Co(II) assemblages. On the contrary, the resulting species do not feature the $[Co(SCN)_4]^{2-}$ unit, instead a neutral mononuclear seven coordinate Mn(II) complex, $[Mn(H_2L)(SCN)_2].4H_2O$ (**1**) was isolated. The inherent soft basic nature of the donor S atom may be attributed for the inability of $[Co(SCN)_4]^{2-}$ in bridging seven coordinated Mn(II) centers. The synthesized compound **1** was characterized with the help of elemental analysis, FT-IR and single crystal X-ray diffraction studies.

Results of the elemental analysis are in good agreement with the proposed formulation of compound **1**. The IR spectrum of compound **1** is depicted in Figure 2.2. Two intense peaks observed at 2094 and 2079 cm^{-1} can be attributed to C≡N stretching vibration of the axial thiocyanate ligands. The IR spectrum features strong absorption bands observed at 1624 cm^{-1} which can be attributed to the C=N stretching vibration of the imine group from the bis-hydrazone ligand. The absorption peak at 1381 cm^{-1} in the spectrum is due the C=C stretching vibration of phenyl rings present in the ligand H_2L. A strong absorption peak was observed at 1537 cm^{-1} and this can be assigned as the stretching frequency due to the phenyl ring of the ligand H_2L.

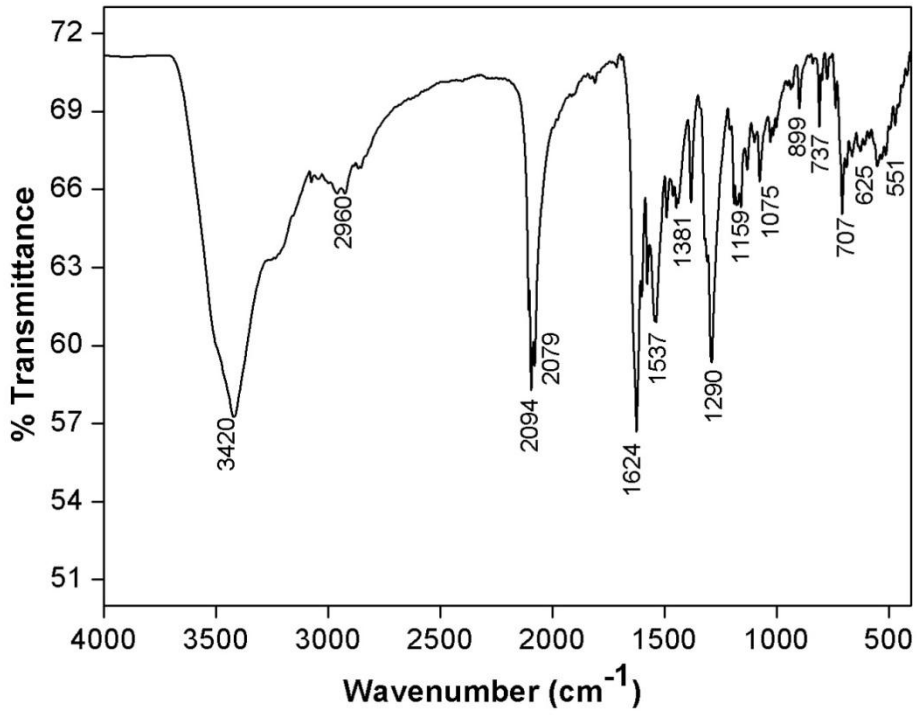

Figure 2.2. FT-IR spectrum of compound **1** as KBr diluted discs

2.3.2. Synthesis and characterization of $[Mn(HL)(H_2O)Cl].2H_2O$ (2)

In recent years, metal-cyanide complexes are gaining considerable interest as they are reported to exhibit tunable magnetic properties. In this regard, approaches have been diverted towards the isolation of cyano-bridged heterometallates that are expected to possess large magnetic anisotropy. The reaction of with $[Mn(H_2L)(H_2O)Cl]Cl$ with equimolar amount of $K_3[Fe(CN)_6]$ is found to be very facile and immediately leads to the formation of a yellow amorphous solid. In order to prevent precipitation of the amorphous solid, we carried out the reaction of $[Mn(H_2L)(H_2O)Cl]Cl$ in methanol with one sixth equivalent of aqueous $K_3[Fe(CN)_6]$ solution in a dilute medium (Scheme 2.2). The solution remained clear for more than a week and orange block shaped crystals are observed after two weeks. However, the expected cyano-bridged complex was not formed and instead the reaction resulted in the formation of $[Mn(HL)(H_2O)Cl].2H_2O$ (**2**) as orange block shaped crystals. The acyclic pentadentate ligand in compound **2** is in mono-anionic form, LH, due to the removal of one N-H proton. It is anticipated that the paramagnetic linker, $[Fe(CN)_6]^{3-}$ used in this reaction has acted as base for the abstraction of protons and this resulted in the isolation of compound **2**.

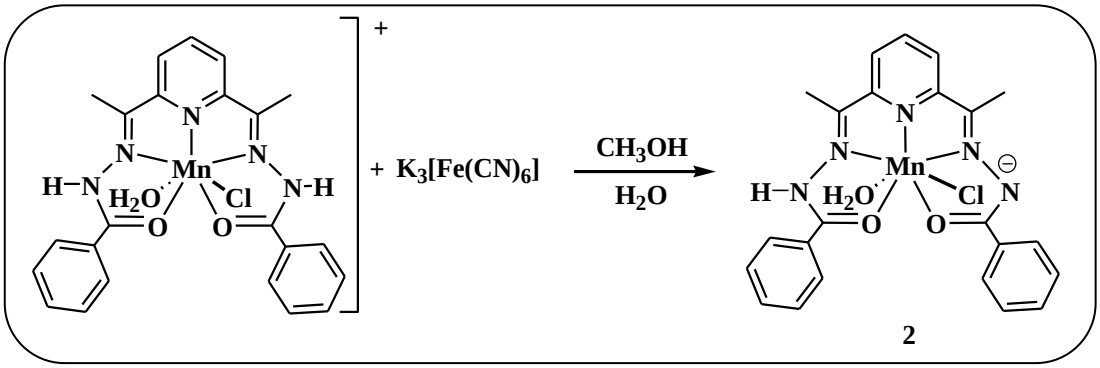

Scheme 2.2. Synthesis of compound **2**

Compound **2** was characterized by using of elemental analysis, FT-IR and single crystal X-ray diffraction studies. The elemental analysis data obtained agrees well with the proposed formulation of compound **2**. The FT-IR spectrum of compound **2** is shown in Figure 2.3. The absorption peak at 1674 cm^{-1} in the IR spectrum of compound **2** can be attributed to the C=N stretching vibration of the imine group from the bis-hydrazone ligand. The absorption peak at 1571 cm^{-1} can be assigned as the stretching frequency due to the phenyl ring of the ligand HL. The absorption peak due to C=C stretching vibration of phenyl rings present in the ligand HL was observed at 1381 cm^{-1}.

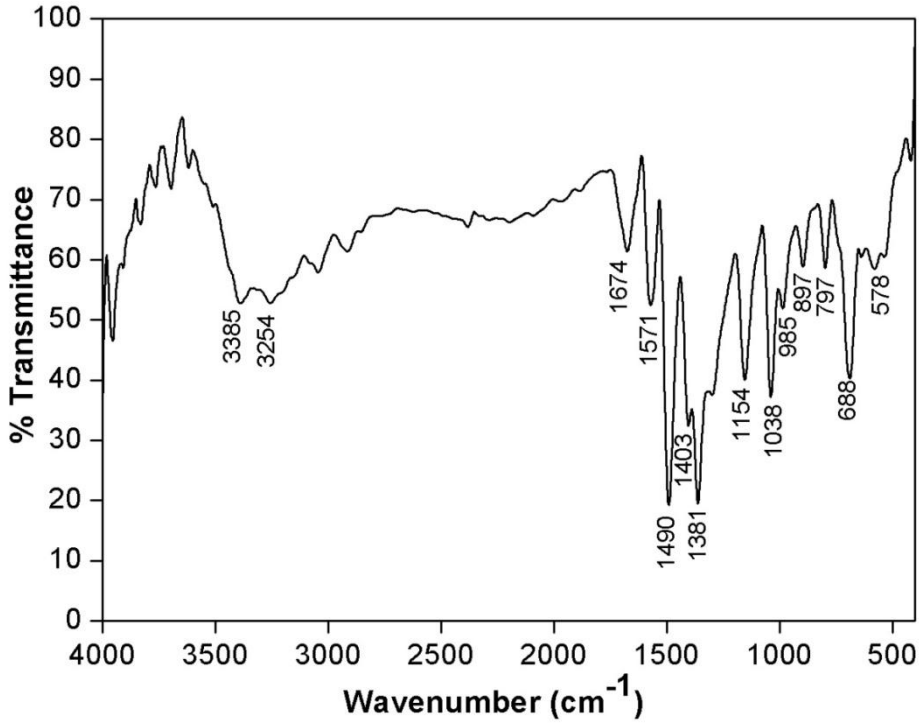

Figure 2.3. FT-IR spectrum of compound **2** as KBr diluted discs

2.3.3. Synthesis and characterization of $[Mn(HL)(H_2O)_2]ClO_4$ (3)

As in the case of compound **2**, similar abstraction of N-H proton to yield mono-anionic acyclic pentadentate ligand can also be facilitated by the ClO_4^- anion. Thus, when the reaction of $[Mn(H_2L)(H_2O)Cl]$ solution in methanol with aqueous $NaClO_4.H_2O$ in stoichiometric ratio was carried out at room temperature, it resulted in the formation of $[Mn(HL)(H_2O)_2]ClO_4$ (**3**) upon slow evaporation of the reaction mixture (Scheme 2.3). The orange needle shaped crystals of compound **3** was characterized by elemental analysis, FT-IR and single crystal X-ray diffraction studies.

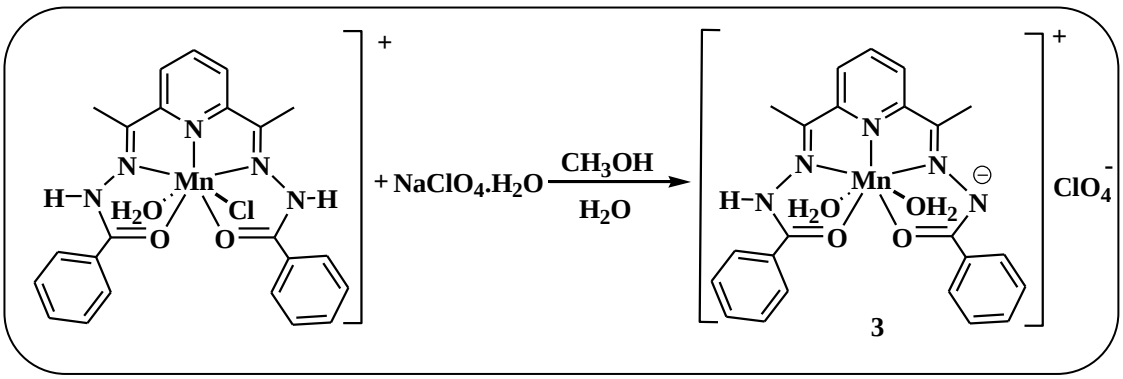

Scheme 2.3. Synthesis of compound **3**

Results of the elemental analysis are in good agreement with that calculated from the proposed formulation of compound **3**. Figure 2.4 depicts the FT-IR spectrum of compound **3**. The FT-IR spectrum of compound **3** shows strong absorption peak at 1620 cm^{-1} which can be attributed to the C=N stretching vibration of the imine group from the bis-hydrazone ligand. The absorption peak at 1532 cm^{-1} can be assigned as the C=C stretching frequency of the phenyl ring present in the ligand HL. The absorption peak observed at 1365 cm^{-1} was due to C=C stretching vibration of phenyl rings present in the ligand HL. The absorption band due to the perchlorate ion is observed at 1088 cm^{-1} in the spectrum.

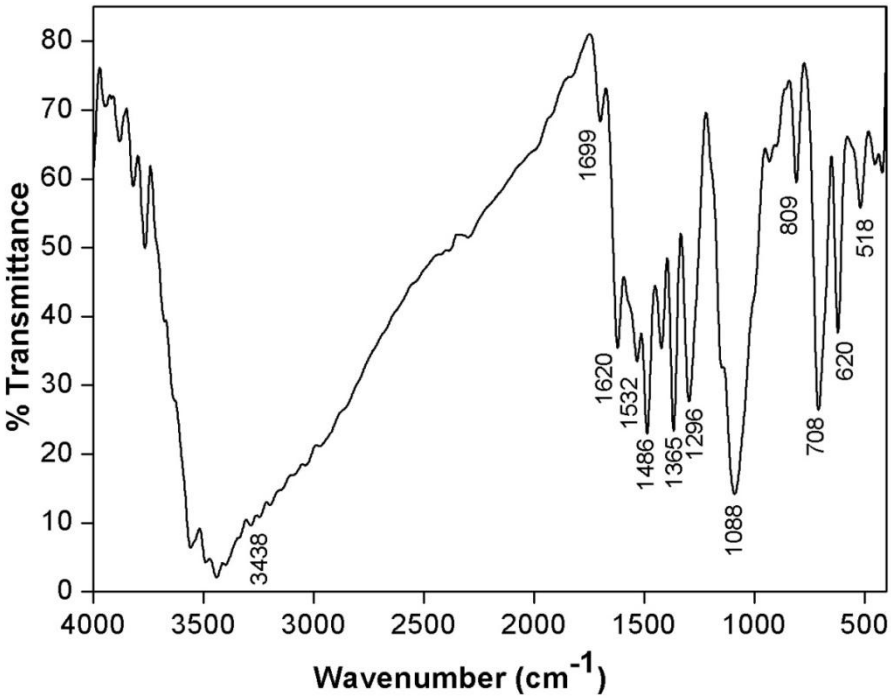

Figure 2.4. FT-IR spectrum of compound **3** as KBr diluted discs

2.3.4. Synthesis and characterization of $[Mn(L)(H_2O)_2]$ (4)

In case of compound **2**, the cyano-bridged architecture was not formed due to very less concentration of $K_3[Fe(CN)_6]$ as it acted as a base in the abstraction of N-H proton. Therefore, the reaction of $[Mn(H_2L)Cl(H_2O)]Cl$ was carried out in presence of excess NaN_3 and equimolar concentration of $K_3[Fe(CN)_6]$. It was anticipated that the ferricyanide may substitute the labile axial sites of the precursor complex, $[Mn(H_2L)Cl(H_2O)]Cl$ and thus result heterometallic Mn(II)-Fe(III) aggregate. However, the reaction yielded a neutral complex $[Mn(L)(H_2O)_2]$ (**4**) where both the N-H protons of the pentadentate ligand are absent (Scheme 2.4). Dark brown block

shaped crystals of compound **4** was isolated and characterized by means of elemental analysis, FT-IR and single crystal X-ray diffraction studies.

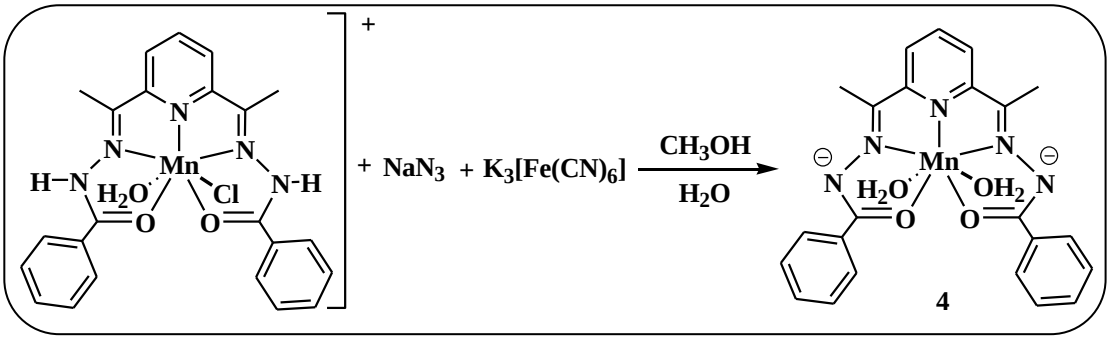

Scheme 2.4. Synthesis of compound **4**

The results found from elemental analysis are in good agreement with that calculated from the proposed formulation of compound **4**. The FT-IR spectrum of compound **4** is given in Figure 2.5. The absorption peak at 1643 cm^{-1} in the IR spectrum of compound **4** can be attributed to the C=N stretching vibration of the imine group from the bis-hydrazone ligand. The absorption peak at 1585 cm^{-1} can be attributed to the stretching frequency of the phenyl ring of the ligand L. The absorbtion peak at 1359 cm^{-1} can be assigned as the absorption peak due to C=C stretching vibration of phenyl rings present in the ligand L.

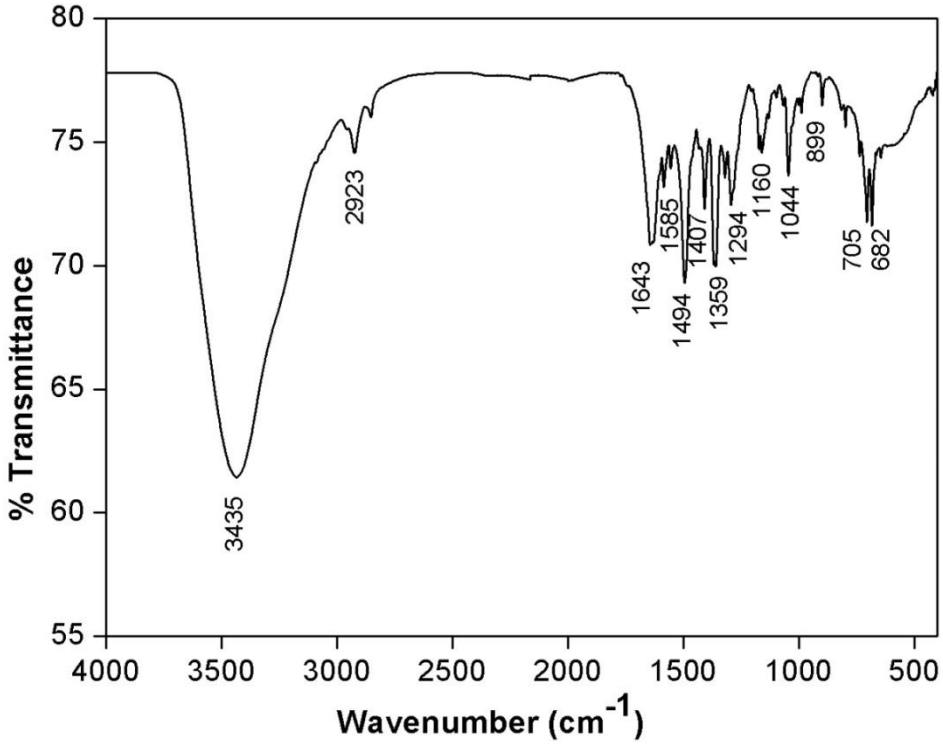

Figure 2.5. FT-IR spectrum of compound **4** as KBr diluted discs

2.3.5. Molecular structures of compounds 1-4

Single crystal X-ray structure of compounds **1-4** have been determined and perspective view of their molecular structures are depicted in Figure 2.6 while relevant crystal data along with refinement parameters are listed in Table 2.2. The pentagonal bipyramidal geometry of the Mn(II) center in the precursor complex, $[Mn(H_2L)(H_2O)Cl]Cl$ is retained in all four new compounds **1-4**. The planer pentadentate bis-hydrazone ligand occupies the equatorial coordination sites in all four mononuclear compounds **1-4**. The pyridine nitrogen atom, two imine nitrogen atoms and two oxygen atoms of the hydrazide moiety from the bis hydrazone ligand are ligated to the Mn(II) centers in compounds **1-4**. In all four compounds, the five donor atoms of the bis hydrazone ligand in are nearly coplanar and the mean deviation from coplanarity are measured as

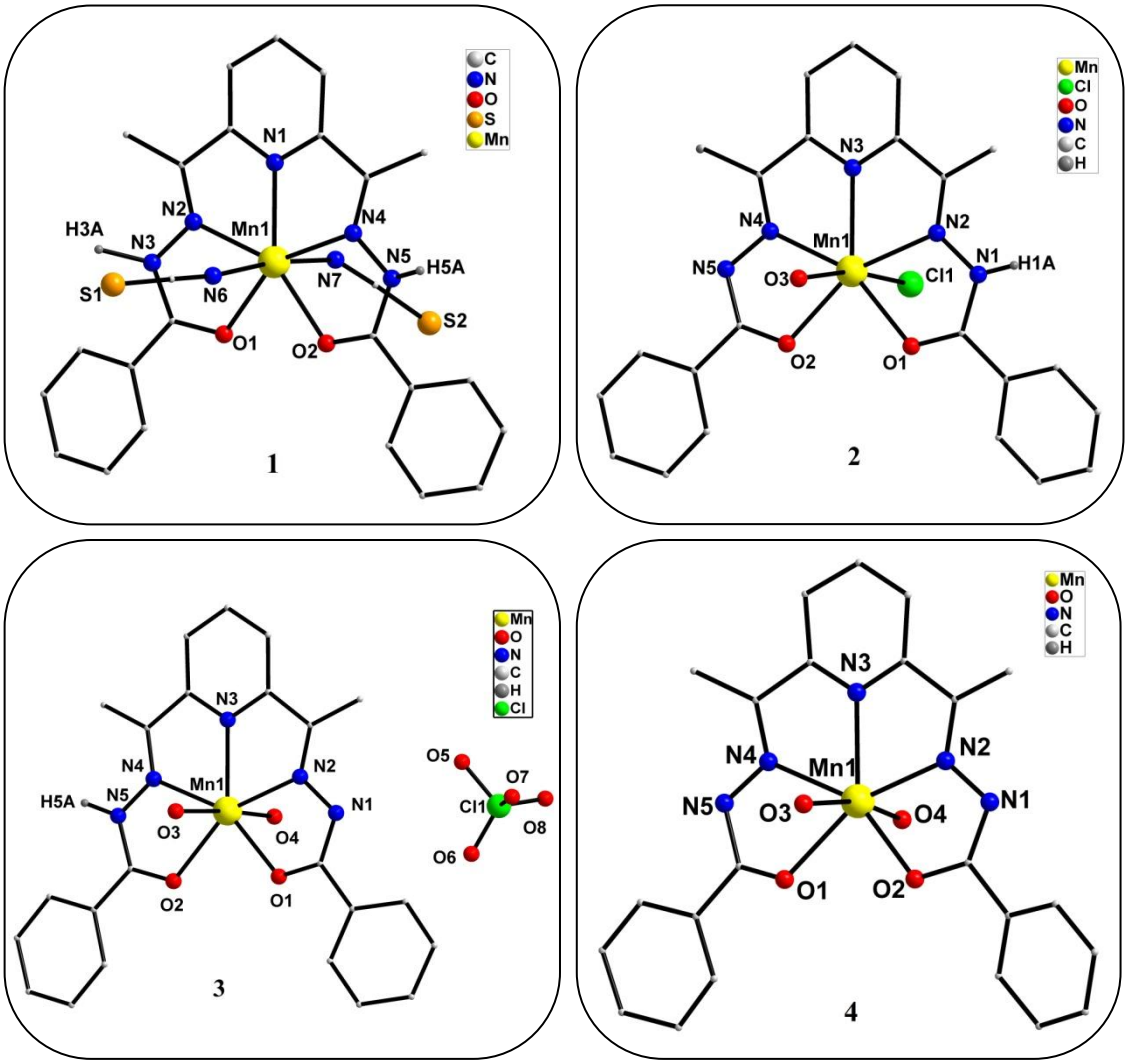

Figure 2.6. Molecular structures of compounds **1-4**. Aromatic and aliphatic hydrogen atoms are omitted for clarity. Only the N-H protons are shown wherever present

0.0952, 0.0462, 0.0304 and 0.000 Å for compounds **1**-**4** respectively. The central Mn(II) centers in compounds **1**-**4** lie 0.0227, 0.1305, 0.0533 and 0.000 Å below the equatorial plane respectively. The sum of the chelate angles and O(1)-Mn(1)-O(2) bite angles in compounds **1**-**4** vary between 359.4-360.5 ° and in all cases lie close to 360°, the sum of angles for an ideal planer structure.

Continuous shape analyses using the SHAPE program reveal (Table 2.1) that for all the four compounds, the mean deviations from D_{5h} pentagonal bipyramidal geometry are least among all possible seven coordinate geometries. Thus, the PBP geometry of the Mn(II) center in the precursor complex, $[Mn(H_2L)(H_2O)Cl]Cl$ has been retained in all the four compounds. Important bond lengths and bond angles of compounds **1**-**4** are listed in Table 2.3.

Table 2.3. Selected bond lengths [Å] and bond angles [◦] of compounds **1**-**4**

Bonds lengths	**1**	**2**	**3**	**4**
Mn-O(1)	2.260(1)	2.256(2)	2.187(3)	2.200(2)
Mn-O(2)	2.229(1)	2.351(2)	2.373(3)	2.342(2)
Mn-N(1)	2.199(1)	2.314(3)	2.256(4)	2.281(2)
Mn-N(2)	2.226(1)	2.366(3)	2.312(3)	2.256(2)
Mn-N(4)	2.221(1)	2.251(2)	2.276(4)	2.327(2)
Mn-axial(1)	2.128(1)	2.504(7)	2.150(3)	2.259(2)
Mn-axial(2)	2.105(1)	2.273(2)	2.187(3)	2.167(2)
Bond Angles	**1**	**2**	**3**	**4**
O(1)-Mn(1)-N(2)	69.84(2)	66.82(6)	69.48(1)	70.25(2)
N(2)-Mn(1)-N(1)	69.63(2)	66.65(9)	69.71(1)	68.77(2)
N(1)-Mn(1)-N(4)	70.10(2)	68.85(8)	68.49(1)	68.45(2)
N(4)-Mn(1)-O(2)	70.18(2)	69.42(7)	66.74(1)	65.70(2)
O(2)-Mn(1)-O(1)	80.80(2)	87.72(6)	87.71(1)	86.82(2)
N(4)-Mn(1)-axial(1)	86.19(1)	87.81(7)	88.47(1)	90.24(2)
N(2)-Mn(1)-axial(2)	84.01(2)	90.96(5)	93.05(1)	95.78(2)
O(1)-Mn(1)-axial(1)	88.92(2)	88.07(5)	90.08(1)	83.31(2)
O(2)-Mn(1)-axial(2)	85.70(2)	79.95(8)	87.71(1)	88.60(2)

Axial(1): SCN(**1**), Cl(**2**), H_2O(**3**), H_2O(**4**); Axial(2): SCN(**1**), H_2O(**2**), H_2O(**3**), H_2O(**4**)

Within the pentadentate bis-hydrazone ligand, the >C=N and N-N bond distances in compound **4** (1.346 Å & 1.480 Å) are found to be relatively longer as compared to respective average bond distances (1.283 Å & 1.383 Å) in compounds **1-3**. Further, C-O bond distances of the hydrazone ligand in compound **1** are shorter (1.229 Å and 1.243 Å) as compared to C-O bond distances observed in compound **4** (1.303 Å). In case of compounds **2** and **3**, one of the C-O bond distances (1.241 & 1.244 respectively) is found to be slightly shorter as compared to the other C-O bond distance (1.275 Å & 1.287 Å respectively).

These intra-ligand bond lengths along with electroneutrality condition for the final complexes establish that the pentadentate bis-hydrazone ligand is present in neutral bis-hydrazine >C=N-NH-C=O form in compound **1**. In compounds **2** and **3**, the bis-hydrazine ligand is present in mono-anionic form as one of the hydrazide arm is present in α-oxiazine >C=N-N=C-O^- while the other arm is present in neutral hydrazine >C=N-NH-C=O form. Both the arms of the bis-hydrazone ligand are present in deprotonated α-oxiazine form in compound **4** and thus it acts as a di-anionic ligand. The equatorial Mn-O bonds distances in compound **1** (2.229 Å and 2.260 Å) are in good agreement with Mn-O bond distances reported for the precursor complex, $[Mn(H_2L)(H_2O)Cl]Cl$ (2.228 Å and 2.278 Å). However, one of the equatorial Mn-O bond distance in compound **2** (2.351 Å) & **3** (2.373 Å) is significantly longer. This can be attributed to the negative charge on the oxygen atom of the deprotonated α-oxiazine arm of the ligand, which strengthens one of the Mn-O bonds. In order to avoid deposition of excess electron density on the central metal center, the other Mn-O bond is elongated considerably. This argument also support the observation that the equatorial Mn-O bond distances in compound **4** (2.297 Å) are found to be equal and comparable to Mn-O bond distances observed in compound **1** as both the arms of the bis-hydrazone ligand are in deprotonated α-oxiazine form. In compound **1**, the axial sites are occupied by nitrogen atoms of two thiocyanato ligands and overall the Mn(II) center has a N_5O_2 coordination environment. The axial Mn-N(thiocyanato) bond distances measure 2.105 Å and 2.128 Å respectively and these bond distances agree well with Mn-N bond distances observed in other thiocyanato complexes. The coordination environment around the central Mn(II) atom in compound **2** is identical to the precursor complex and while the Mn-Cl distances in both the compounds measure 2.503 Å, the axial Mn-O(H_2O) distance in compound **2** (2.273 Å) is slightly longer as compared to that in the

precursor complex (2.258 Å). Compounds **2** and **3** show interesting hydrogen bonding architecture due to the presence of lattice water molecules. The structural parameters of all hydrogen bonds observed in compounds **2** and **3** are listed in Table 2.4.

Table 2.4. Hydrogen bonding parameters of compounds **2** and **3**

Complex	**Interactions**	**H···A (Å)**	**D···A (Å)**	**∠D–H···A(°)**	**Symmetry**
2	O(3)-H(3A)...O(2)	2.610	2.910(3)	104.0	1-x, 1-y, 1-z
	O(3)-H(3B)...O(1)	2.870	3.100(3)	99.0	1-x, 1-y, 1-z
3	O(4)-H(4A)...O(1)	2.910	3.051(4)	92.0	1-x, -y, 1-z
	O(4)-H(4B)...O(2)	2.880	3.074(4)	95.0	1-x, -y, 1-z
	N(5)-H(5A)...O(7)	2.340	3.027(6)	134.0	1-x, 1-y, -z
	O(3)-H(3A)...O(5)	1.995	2.812(4)	163.0	1-x, 1-y, -z

In case of compound **2**, there are two lattice water molecules in each asymmetric unit. These two lattice water molecules are involved in strong O-H···O hydrogen bonding with lattice water molecules of a nearby asymmetric unit. This leads to the formation of a hydrogen bonded cyclic water tetramer (Figure 2.7). The structure of the water tetramer present in compound **2** is depicted in Figure 2.8. It has an irregular uudd configuration [47]. Within the water tetramer, all atoms participating in O-H···O hydrogen bonding (four hydrogen atoms and all four oxygen atoms) reside in one plane. The remaining four hydrogen atoms which do not participate in intra-tetramer hydrogen bonding interactions protrude out of the above plane. The uudd configuration is not the most stable mode of cyclic water tetramer and very few examples of uudd water tetramer has been reported so far [47-51].

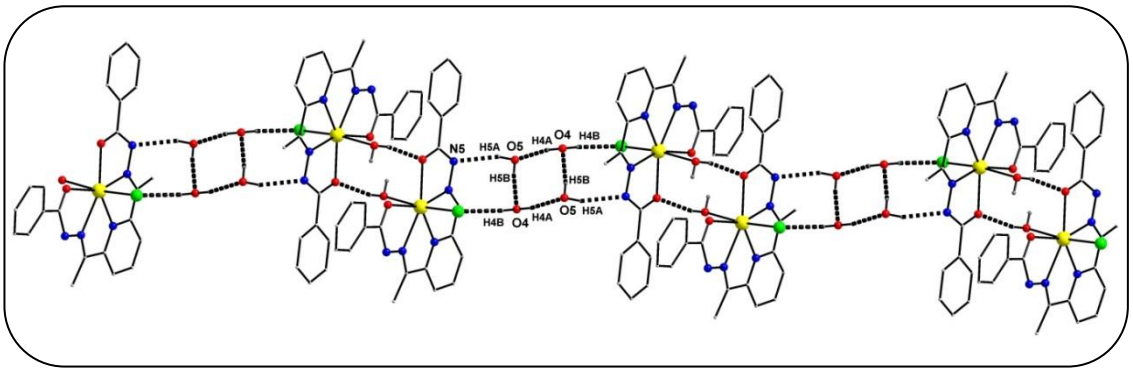

Figure 2.7. Hydrogen bonding pattern of compound **2**

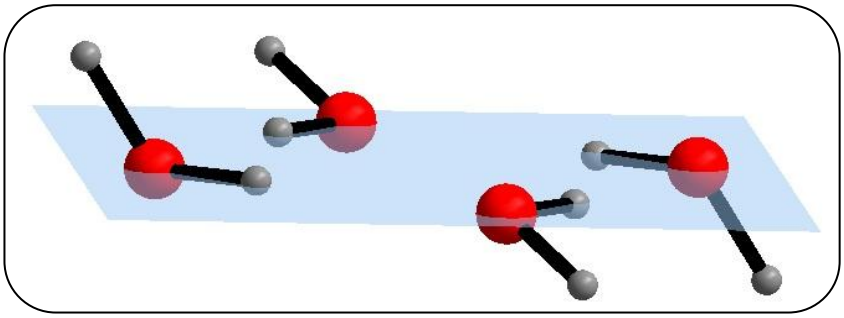

Figure 2.8. Water tetramer formed in compound **2**

Both the hydrogen atoms from one of the water coordinated to the Mn(II) center form strong hydrogen bonding with equatorial oxygen atoms of a nearby molecule. This leads to the formation of a hydrogen bonded dimeric structure in compound **2**. Further, the four exocyclic hydrogen atoms of the water tetramer are involved in O-H···Cl hydrogen bonding with the axially coordinated chloro ligand and O-H···N hydrogen bonding with the deprotonated nitrogen atom of the pentadentate ligand. This leads to the formation of a ladder shaped 1D supramolecular chain structure as shown in Figure 2.8. The donor-acceptor bond distances within the water tetramer are 2.837 (2) Å and 2.800 (3) Å and compare well with the donor-acceptor distances in udud water tetramers reported earlier.

In compound **3**, no lattice water molecules are present and therefore the supramolecular hydrogen bonded architecture observed is largely due to involvement of the two H_2O coordinated at the axial site of the Mn(II) center. Both hydrogen atoms from one of the axial H_2O i.e., O(4) form strong O-H···O hydrogen bonding with the two oxygen atoms, O(1) and O(2) occupying equatorial sites of a nearby molecule as shown in Figure 2.9. This leads to the formation of a hydrogen bonded dimeric structure. Further, one of the H-atom (H3B) attached to the other axial H_2O (O3) form strong O-H···N hydrogen bonding with the deprotonated nitrogen atom N(5) of the α-oxiazine ligand in a nearby molecule. This leads to the formation of a 1D hydrogen bond network in compound **3**. The perchlorate ions are also involved in hydrogen bonding and embedded between the 1D supramolecular networks. The remaining H atom of the axial H_2O i.e., O(3) forms hydrogen bond with the O(5) atom of the perchlorate ion present in the lattice. Both compounds **2** and **3**, one of the axial H_2O is hydrogen bonded with equatorial oxygen atoms of a nearby molecule and this leads to the formation of a dimeric structure.

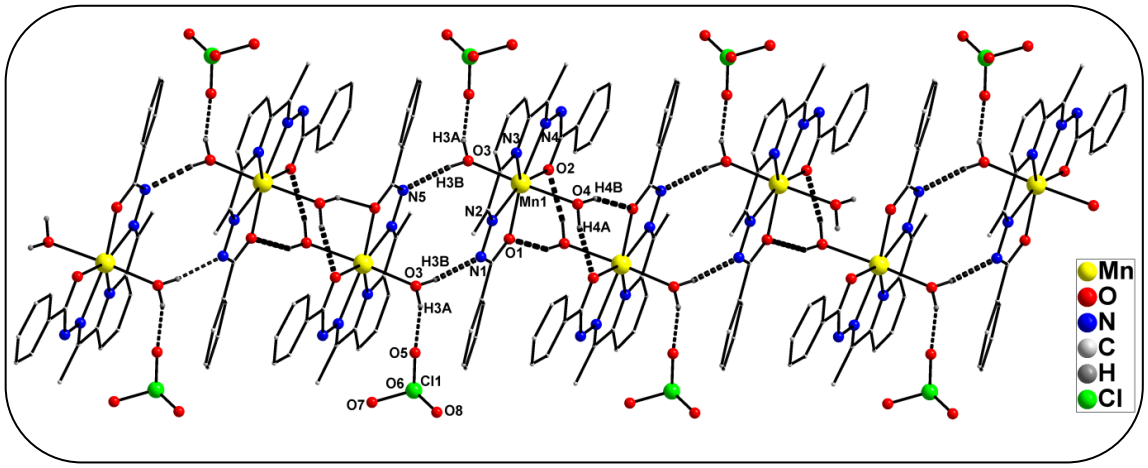

Figure 2.9. Hydrogen bonding pattern of compound **3**

2.3.6. Superoxide dismutase activity

The superoxide scavenging activity of the mononuclear Mn(II) compounds **1-4** were investigated by employing a modified nitro blue tetrazolium (NBT) assay. The indirect determination of SOD activity was monitored by the reduction of NBT by superoxide

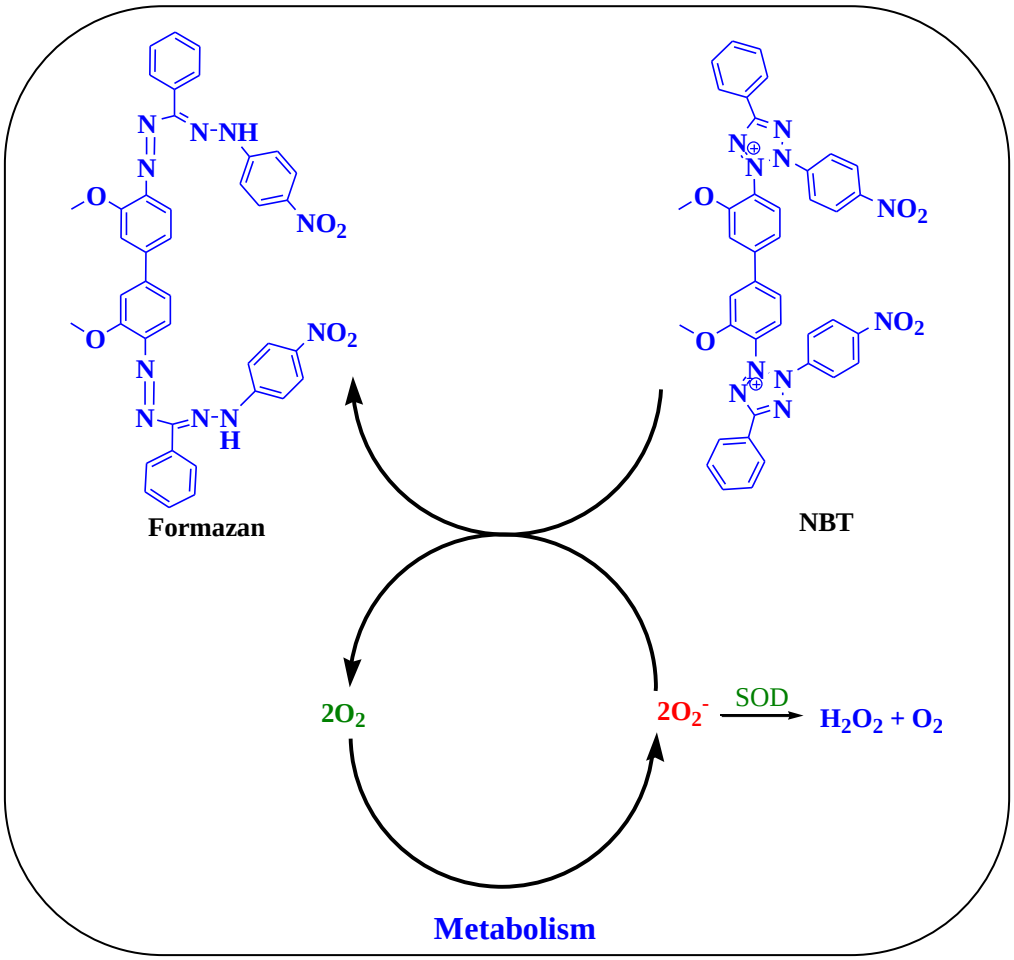

Scheme 2.5. Probable mechanism for the reduction of NBT by superoxide

generated by alkaline DMSO. As the reaction proceeds, the colour of the solution changes from light yellow to blue due to the formation of blue formazan. This blue coloured formazan dye formed can be detected spectrophotometrically. The probable mechanism for reduction of NBT by superoxide is depicted in Scheme 2.5.

Compounds **1** and **2** do not show any superoxide dismutase activity. In contrast, compounds **3** and **4** are catalytically active towards dismutation of superoxide. The IC_{50} values of the compounds **3** and **4** are calculated to be 1.18 and 2.10 µM respectively (Figure 2.10). These values signify that compound **4** acts as a better SOD mimic. This indicates that the presence of labile aqua-ligands in the axial coordination of the metal complexes is the essential criteria for the SOD catalysis.

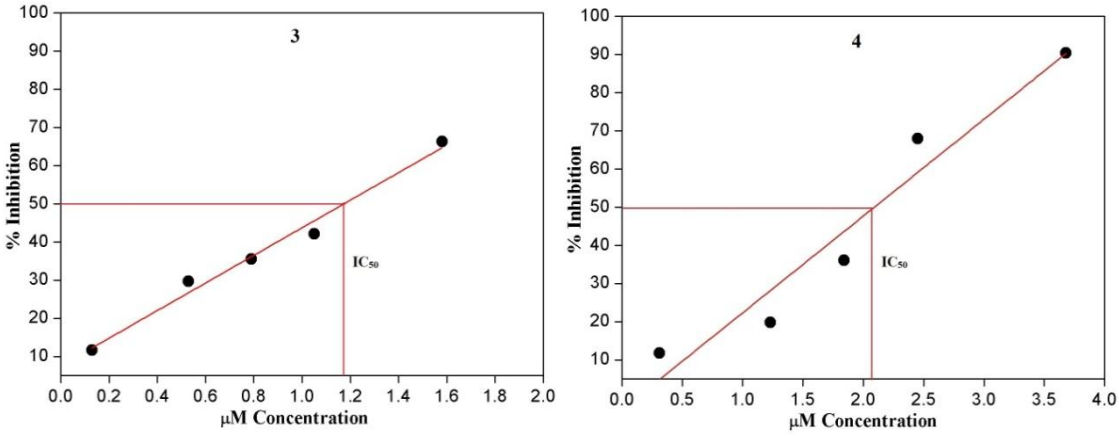

Figure 2.10. Determination of IC_{50}: Inhibition percentage as a function of the concentrations of compounds **3** and **4** respectively

The SOD activities were determined as their IC_{50} values and a systematic comparison of the IC_{50} values of the reported seven coordinated Mn(II) complexes in PBP geometry have been depicted in Table 2.5. The IC_{50} values of compounds **3** and **4** are found to be considerably high as compared to the native MnSOD complex. However, the IC_{50} values of compounds **3** and **4** are comparable to those observed in case of acyclic PBP Mn(II) complexes reported earlier.

Table 2.5. IC_{50} values of mononuclear Mn(II) complexes

Sl.No.	Complexes	IC_{50} value	References
1.	Native MnSOD	0.005	53
2.	$[Mn(L_1)(CH_3OH)(H_2O)(ClO_4)(H_2O)]$	0.013	28
3.	$[Mn(Me_2[15]pyridinane\ N_5)(H_2O)_2]Cl_2.H_2O$	0.024	28
4.	$[Mn(L_2)(OTf)_2]$	0.75	27
5.	$[Mn(L_3)(OTf)_2]$	1.41	27
6.	$[Mn(L_4)(OTf)_2]$	1.51	27
7.	$[Mn(L_4)Cl_2]$	2.57	27
8.	$[Mn(H_2L)(SCN)_2].4H_2O$ (**1**)	Not active	This work
9.	$[Mn(HL)(H_2O)Cl].2H_2O$ (**2**)	Not active	This work
10.	$[Mn(HL)(H_2O)_2]ClO_4$ (**3**)	1.18	This work
11.	$[Mn(L)(H_2O)_2]$ (**4**)	2.10	This work

L_1: 2,6-diacetylpyridinebis(semioxamazide); L_2: 2,6-bis(pyridine-2-methyl sulfanylmethyl)-pyridine; L_3: 2,6-bis(pyridine-2-yl methoxymethyl)-pyridine; L_4: pyrridin-2-yl methyl-(6{[pyridine-2-yl methyl]-methyl}pyridine-2-yl methyl)-amine; H_2L: 2,6-diacetylpyridinebis(benzoyl hydrazone)

2.3.7. Variable temperature magnetic studies of compounds 1-4

Magnetization measurements were performed on the polycrystalline samples of compounds **1-4**. Temperature dependence of magnetic susceptibility of compounds **1-4** were measured under an applied field of 1000 K and Figure 2.11 depicts the variation of $\chi_M T$ between 2-300 K for compounds **1-4**. The $\chi_M T$ products at 300 K are found to be 4.51, 4.56, 4.76 and 4.65 cm^3Kmol^{-1} for compounds **1-4** respectively. These values are slightly higher than the expected $\chi_M T$ product of 4.375 cm^3Kmol^{-1} for a magnetically isolated Mn(II) center considering S = 5/2 and g = 2.0. On lowering the temperature, the $\chi_M T$ product remains constant upto 56 K for compound **1** and on further lowering, $\chi_M T$ decreases to reach 3.027 cm^3Kmol^{-1} at 2 K. However, for compounds **2** and **3**, the $\chi_M T$ product remains static upto 7 K and 5 K respectively. On further lowering the temperature, the $\chi_M T$ product for compounds **2** and **3** decreases abruptly upto 3.74 and 3.99 cm^3Kmol^{-1} respectively. The decrease in $\chi_M T$ product at much higher temperature for compound **1** as compared to compounds **2** and **3** can be either attributed to hydrogen bonding mediated antiferromagnetic interactions or

relatively larger zero field splitting in compound **1**. In compound **4**, the $\chi_M T$ product remains constant upto 26 K on lowering the temperature and, $\chi_M T$ decreases to reach 3.69 cm^3Kmol^{-1} on further lowering to 2 K.

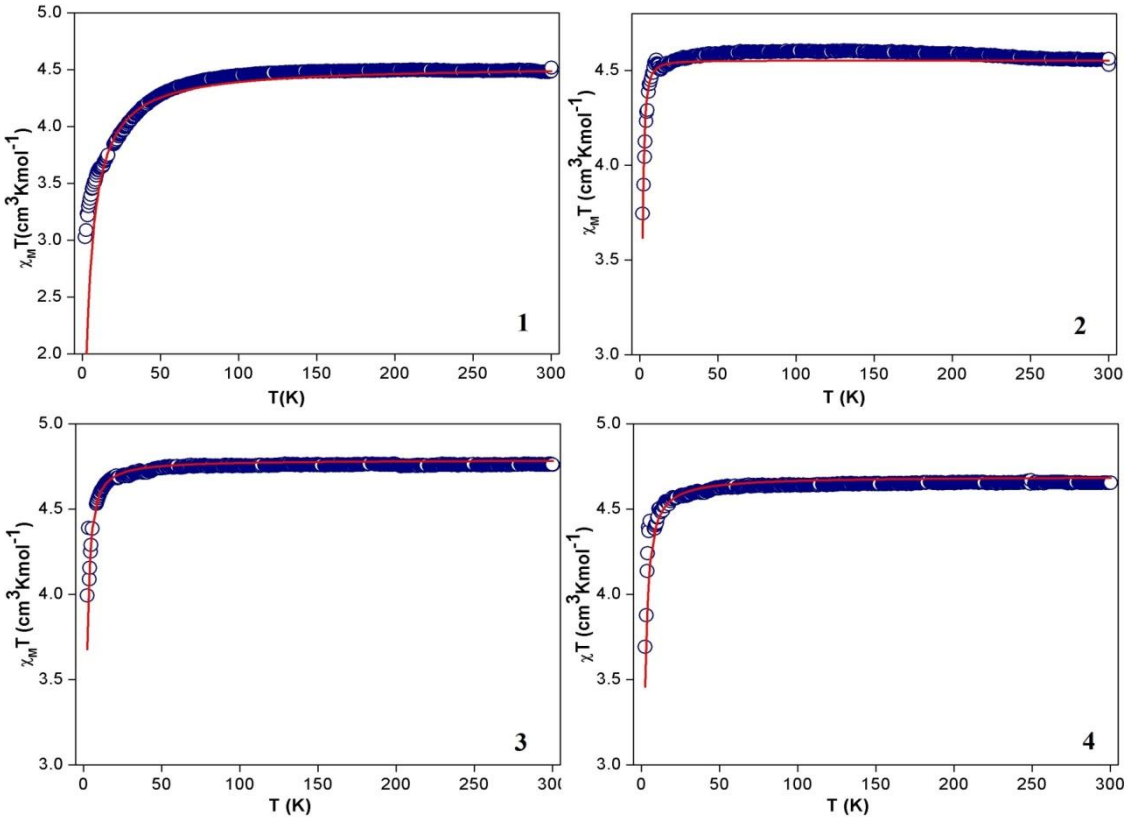

Figure 2.11. Temperature dependence of $\chi_M T$ between 2-300 K for compounds **1-4** respectively. The circles represent experimental data and the solid lines indicate the best fit obtained by using PHI program

Temperature dependence of $1/\chi_M$ between 5-300 K of compounds **1-4** is depicted in Figure 2.12. All the three compounds obey Curie-Weiss law with a Weiss constant θ = 1.66 K, -0.61 K, 0.61 K and -1.39 K respectively for compounds **1-4**. The Curie constant C equals 4.47 cm^3Kmol^{-1}, 4.45 cm^3Kmol^{-1}, 4.78 cm^3Kmol^{-1} and 4.173 cm^3Kmol^{-1} for compounds **1-4** respectively. The experimental C value agrees well with the calculated C value of 4.375 cm^3Kmol^{-1} for an isolated high spin Mn(II) with S = 5/2 assuming g_{Mn}= 2.0. The sign of Weiss constant indicates the presence of weak ferromagnetic interactions between the spin carriers in case of compounds **1** and **3**, whereas weak antiferromagnetic interaction due to hydrogen bonding prevail in compounds **2** and **4**.

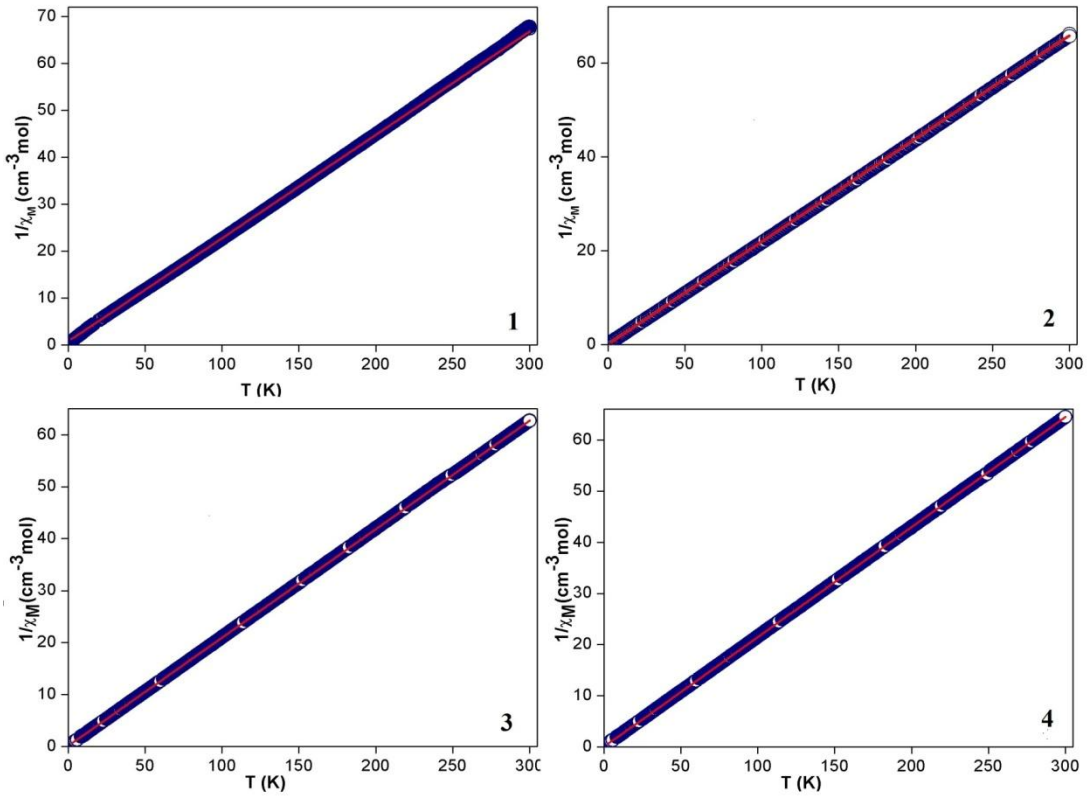

Figure 2.12. Variation of $1/\chi_M$ against temperature for compounds **1**-**4**. Circles represent experimental value and the solid line represents the best fit obtained by using PHI program

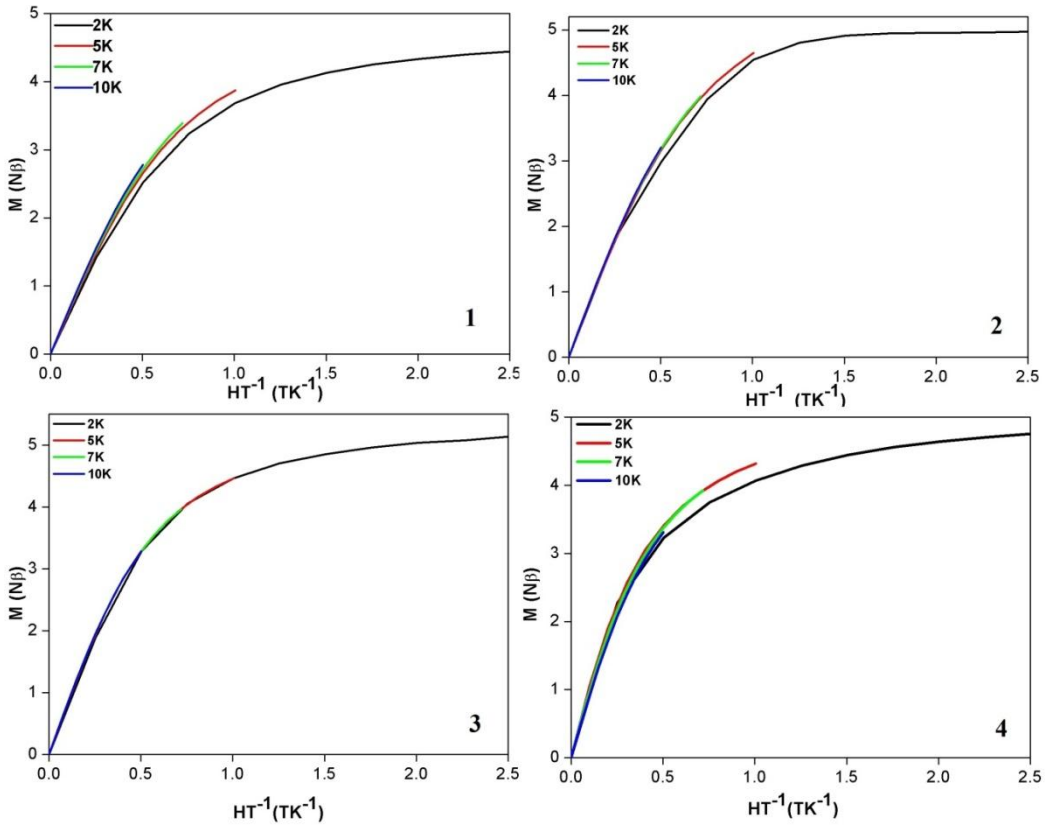

Figure 2.13. Reduced magnetization plots of compounds **1**-**4** respectively

The reduced magnetization plots for compounds **1-4** are depicted in Figure 2.13. For compound **1**, **2** and **3**, the reduced magnetization plots at different temperatures do not completely superimpose on each other and this indicate that the presence of magnetic anisotropy in the mononuclear Mn(II) complexes. However, in case of compound **3**, reduced magnetization plots at different temperatures superimpose on each other and this rules out the presence of magnetic anisotropy in compound **3**.

Isothermal field dependence of magnetization for compounds **1-4** was measured between 2-10 K are depicted in Figure 2.14. Magnetization increases linearly with the increase in field strength for all these compounds, but saturation magnetization M_s= 5 μB (for S = 5/2 and g = 2.0) was not achieved even at a field strength of 5 T for compounds **1-4**.

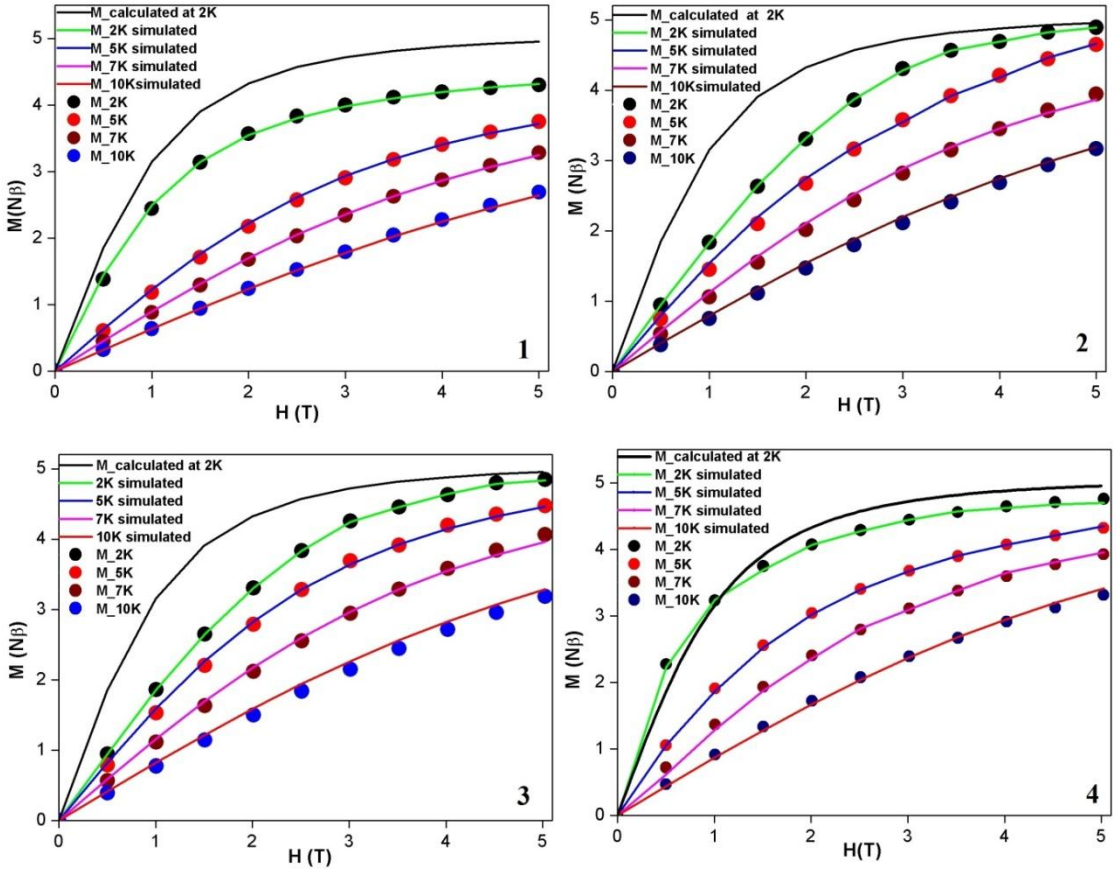

Figure 2.14. Field dependence of magnetization between 0-5 T for compounds **1-4** respectively along with the calculated magnetization behaviour for an isotropic S=5/2 system. Circles represent experimental value and the solid lines are the best fit obtained by using PHI program

A spin Hamiltonian of equation 1 can be utilized to qualitatively describe zero field splitting:

$$\hat{H} = D/3\ \hat{O}_2^0 + E\hat{O}_2^2 + g\mu_B\hat{S} \times B \qquad (1)$$

where, μ_B, E, $\hat{S}$ and B represent Bohr magneton, rhombic ZFS parameter, spin and magnetic field vectors respectively while $\hat{O}_k^q$ is the equivalent operator as described by Stevens [43]. The ZFS parameters in compounds **1**-**3** were evaluated by least square fitting of the field dependence of magnetization plots. Initially, temperature dependence of the $\chi_M T$ plot was fitted by using the PHI program and it lends the value of *g* parameter as 2.03, 2.02, 2.05 and 2.05 for compounds **1**-**4** respectively. Best fitting of the field dependence of magnetization plots by using the above g parameters yielded the value of D parameters as 0.606, 0.201, 0.010 and -0.88 cm^{-1} respectively for compounds **1**-**4**. As anticipated from the reduced magnetization plots, the D value for compound **1** is significantly larger as compared to the D value of compound **2** while the D value obtained for compound **3** is very close to zero. Moreover, the D value is small negative in compound **4**.

In order to theoretically estimate the ZFS parameters in compounds **1**-**4** and also to unravel the origin of ZFS in PBP Mn(II) complexes, DFT calculations were also performed by using the Coupled Perturbed (CP) method as implemented in ORCA module [52]. The results of the CP calculations are summarized in Table 2.6 and very good agreement between the experimentally evaluated D parameters with the CP method calculated values are observed for all compounds. DFT calculations show that the spin-spin (SS) interaction between the unpaired electrons (1^{st} order perturbation) along with the spin orbit coupling (SOC) of the electronically excited states with the ground states (2^{nd} order perturbation) contributes to the ZFS. Moreover, it is observed that major contribution to the axial ZFS parameter, D comes from SOC for compounds **1** and **2**. However, for compound **3**, a significant contribution to the overall D value

Table 2.6. Data obtained from ORCA program for compounds **1**-**4**

Complex	$\mathbf{D_{exp}}$	$\mathbf{D_{calc}}$	**E/D**	**Dssc**	$\mathbf{D_{SOC}}$	**α→α**	**β→β**	**α→β**	**β→α**
1	0.60	0.506	0.162	0.003	0.503	-0.092	0.005	0.587	0.003
2	0.20	0.192	0.081	0.009	0.183	0.067	0.026	0.119	-0.029
3	0.002	-0.071	0.232	-0.025	-0.046	-0.001	-0.024	-0.028	0.008
4	-0.88	-0.746	0.320	-0.076	-0.670	0.089	-0.004	-0.231	-0.524

comes from spin-spin coupling between the five d-electrons present in Mn(II). The DFT calculated sign of the D parameter obtained for compounds **1**, **2** and **4** agree with the experimental D values, but it do not match for compound **3.** This discrepancy in the sign of D parameter can be attributed to unreliability of DFT calculated D parameter in seven coordinated complexes when the value of E/D is found to be greater than 0.19.

High spin Mn(II) complexes are expected to be isotropic in any coordination environment and the ZFS parameter should be very small. ZFS parameter of a large number of six and five coordinate Mn(II) complexes have been probed and D values ranging between 0.0009-1.46 have been reported. However, systematic investigation of ZFS parameters in seven coordinated Mn(II) complexes are relatively scarce and so far D values have been reported only for four PBP complexes [26-27]. Results described herein allow us to unravel the influence of subtle coordination environment modifications on the ZFS parameters. Substituting one of the axial H_2O ligand in compound **3** with a chloro ligand in compound **2**, leads to significant enhancement of the overall D parameter. Careful inspection of Table 2.6 reveals that apart from the $\beta\rightarrow\beta$ excitation, contributions from all other excitations are significantly large in case of compound **2**. Due to increase in axial ligand field strength in compound **2**, better interference of the metal electrons with the ligand electrons are expected and this leads to eventual increase in D_{SOC}. A similar trend is also observed when axial ligand field strength is further increased by substituting both the axial sites by thiocyanato ligand as in compound **1**. Substantial increase in D_{SOC} is observed as contribution of $\alpha\rightarrow\beta$ excitation is enhanced and it further establishes the interplay of ligand field strength in D_{SOC}. In compound **4**, the equatorial ligand field strength is enhanced while the axial ligand field strength is weakened by the H_2O ligand. All the contributions are negative except that of $\alpha\rightarrow\ \alpha$ excitation, thereby leading to a overall negative value of D in compound **4**.

2.4. Conclusions

Thus, a series of PBP Mn(II) complexes have been prepared by using a planar pentadentate bis-hydrazone ligand and all the complexes were characterized with the aid of analytical, spectroscopic and structural tools. Single crystal X-ray structure determinations of all four complexes, **1**-**4** reveal that the coordination environments of the four complexes are subtly different from each other. The acyclic pentadentate bis

hydrazone ligand H_2L is neutral in compound **1** while in compounds **2** and **3**, it is monoanionic. The dianionic form of the ligand is observed in compound **4**. The zero field splitting parameters of compounds **1**-**4** have been determined both experimentally and theoretically. In general, good agreement is observed between the experimentally determined ZFS parameter and theoretically estimated ZFS parameters. Results presented herein indicate that the value of ZFS in PBP Mn(II) complexes strongly depend on the coordination environment. As observed for five and six coordinate Mn(II)-halide complexes, the ZFS of PBP Mn(II) complexes also increase with increasing covalency of axial metal-ligand bond. In spite of identical equatorial ligand environment in both compounds **2** and **3**, the large difference in ZFS between these two compounds can be attributed to the larger covalency of Mn(II)-chloride bond in compound **2** as compared to Mn(II)-O(H_2O) bond in **3**. Accordingly, presence of two Mn(II)-NCS bond with reasonable covalency accounts for the rather large ZFS observed in compound **1**. However, the ZFS value observed in compound **4** is large and negative and therefore cannot be accounted by the covalency of axial metal-ligand bond. The pentadentate equatorial ligand in compound **4** is present dianionic state and therefore the covalency of equatorial metal-ligand bonds are high which eventually leads to a large negative ZFS. Further, it has been also observed that modulation of the axial and equatorial field strength affects the value of D in these mononuclear Mn(II) complexes. The values of D in compounds **2** and **3** decrease with the decrease of the axial field strength as compared to that of compound **1**. On further strengthening of the equatorial field strength while lowering that of the axial field strength, the value of D reaches to a minimum value in compound **4**.

The SOD activity of the rigid pentagonal bipyramidal systems, compounds **1**-**4** has been evaluated by using an indirect assay and it is observed that compounds **3** and **4** can efficiently decompose superoxide. Moreover, compound **3** shows better SOD activity than compound **4**. Thus, the results presented herein show that presence of labile aquo ligand coordinated to the PBP Mn(II) center is the most important prerequisite for observing SOD activity. The IC_{50} values observed for compounds **3** & **4** are far higher than those reported for native MnSOD or macrocyclic PBP Mn(II) complexes. However, the IC_{50} values of compounds **3**-**4** are comparable to those observed in case of acyclic Mn(II) complexes reported earlier.

2.5. References

[1] Larson, E. J., and Pecoraro, V. L. *Manganese Redox Enzymes*, V. L. Pecoraro., Ed., VCH Publishers, New York, 1-2, 1992.

[2] Dismukes, G. C. Manganese enzymes with binuclear active sites. *Chemical Reviews*, 96(7): 2909-2926, 1996.

[3] Yachandra, V. K., Sauer, K., and Klein, M. P. Manganese cluster in photosynthesis: where plants oxidize water to dioxygen. *Chemical Reviews*, 96(7): 2927-2950, 1996.

[4] Farrell, N. P. *Uses of Inorganic Chemistry in Medicine*, The Royal Society of Chemistry Publishers, Cambridge, U. K., 1999.

[5] Iranzo, O. Manganese complexes displaying superoxide dismutase activity: a balance between different factors. *Bioorganic chemistry*, 39(2): 73-87, 2011.

[6] Riley, D. P., and Schall, O. F. Structure–activity studies and the design of synthetic superoxide dismutase (SOD) mimetics as therapeutics. *Advances in Inorganic Chemistry*, 59: 233-263, 2006.

[7] Giblin, G. M., Box, P. C., Campbell, I. B., Hancock, A. P., Roomans, S., Mills, G. I., and Huffman, K. 6, 6′-Bis (2-hydroxyphenyl)-2, 2′-bipyridine manganese (III) complexes: A novel series of superoxide dismutase and catalase mimetics. *Bioorganic & Medicinal Chemistry Letters*, 11(11): 1367-1370, 2001.

[8] Doctrow, S. R., Huffman, K., Marcus, C. B., Tocco, G., Malfroy, E., Adinolfi, C. A., and Malfroy, B. Salen-manganese complexes as catalytic scavengers of hydrogen peroxide and cytoprotective agents: structure-activity relationship studies. *Journal of Medicinal Chemistry*, 45(20): 4549-4558, 2002.

[9] Salvemini, D., Wang, Z. Q., Zweier, J. L., Samouilov, A., Macarthur, H., Misko, T. P., and Riley, D. P. A nonpeptidyl mimic of superoxide dismutase with therapeutic activity in rats. *Science*, 286(5438): 304-306, 1999.

[10] Smoukov, S. K., Telser, J., Bernat, B. A., Rife, C. L., Armstrong, R. N., and Hoffman, B. M. EPR study of substrate binding to the Mn (II) active site of the bacterial antibiotic resistance enzyme FosA: a better way to examine Mn (II). *Journal of the American Chemical Society*, 124(10): 2318-2326, 2002.

[11] Duboc, C., Astier-Perret, V., Chen, H., Pécaut, J., Crabtree, R. H., Brudvig, G. W., and Collomb, M. N. A multifrequency high-field EPR (9–285GHz) investigation of a series of dichloride mononuclear penta-coordinated Mn(II)

complexes. *Inorganica Chimica Acta*, 359(5): 1541-1548, 2006 and references therein.

[12] Duboc, C., Collomb, M. N., and Neese, F. Understanding the zero-field splitting of mononuclear manganese (II) complexes from combined EPR spectroscopy and quantum chemistry. *Applied Magnetic Resonance*, 37(1-4): 229-245, 2010.

[13] Birdy, R. B., and Goodgame, M. Electron spin resonance study of manganese (II) ions in $M(N_2H_4)_2X_2$. *Inorganica Chimica Acta*, 50: 183-187, 1981.

[14] Jacobsen, C. J., Pedersen, E., Villadsen, J., and Weihe, H. ESR characterization of trans-diacidatotetrakis (pyridine) vanadium and-manganese trans-$V^{II}(py)_4X_2$ and trans-$Mn^{II}(py)_4X_2$ (X=NCS, Cl, Br, I; py= pyridine). *Inorganic Chemistry*, 32(7): 1216-1221, 1993.

[15] Lynch, W. B., Boorse, R. S., and Freed, J. H. A 250-GHz ESR study of highly distorted manganese complexes. *Journal of the American Chemical Society*, 115(23): 10909-10915, 1993.

[16] Wood, R. M., Stucker, D. M., Jones, L. M., Lynch, W. B., Misra, S. K., and Freed, J. H. An EPR study of some highly distorted tetrahedral manganese (II) complexes at high magnetic fields. *Inorganic Chemistry*, 38(23): 5384-5388, 1999.

[17] Goodgame, D. M., El Mkami, H., Smith, G. M., Zhao, J. P., and McInnes, E. J. High-frequency EPR of octahedral Mn(II) compounds with large zero-field splittings. *Dalton Transactions*, 34-35, 2003.

[18] Mantel, C., Baffert, C., Romero, I., Deronzier, A., Pécaut, J., Collomb, M. N., and Duboc, C. Structural characterization and electronic properties determination by high-field and high-frequency EPR of a series of five-coordinated Mn(II) complexes. *Inorganic Chemistry*, 43(20): 6455-6463, 2004.

[19] Mantel, C., Philouze, C., Collomb, M. N., and Duboc, C. Investigation of a Neat versus Magnetically Diluted Powdered Mononuclear Mn^{II} Complex by High-Field and High-Frequency EPR Spectroscopy. *European Journal of Inorganic Chemistry*, 2004(19): 3880-3886, 2004.

[20] Käss, H., MacMillan, F., Ludwig, B., and Prisner, T. F. Investigation of the Mn binding site in cytochrome c oxidase from Paracoccus denitrificans by high-frequency EPR. *The Journal of Physical Chemistry B*, 104(22): 5362-5371, 2000.

[21] Un, S., Tabares, L. C., Cortez, N., Hiraoka, B. Y., and Yamakura, F. Manganese(II) zero-field interaction in cambialistic and manganese superoxide dismutases and its relationship to the structure of the metal binding site. *Journal of the American Chemical Society*, 126(9): 2720-2726, 2004.

[22] Kappl, R., Ranguelova, K., Koch, B., Duboc, C., and Hüttermann, J. Multi-frequency high-field EPR studies on metal-substituted xylose isomerase. *Magnetic Resonance in Chemistry*, 43(S1): S65-S73, 2005.

[23] Duboc, C., Phoeung, T., Zein, S., Pécaut, J., Collomb, M. N., and Neese, F. Origin of the zero-field splitting in mononuclear octahedral dihalide Mn^{II} complexes: An investigation by multifrequency high-field electron paramagnetic resonance and density functional theory. *Inorganic Chemistry*, 46(12): 4905-4916, 2007 and references therein.

[24] Rich, J., Castillo, C. E., Romero, I., Rodríguez, M., Duboc, C., and Collomb, M. N. Investigation of the Zero-Field Splitting in Six-and Seven-Coordinate Mononuclear MnII Complexes with N/O-Based Ligands by Combining EPR Spectroscopy and Quantum Chemistry. *European Journal of Inorganic Chemistry*, 2010(23): 3658-3665, 2010.

[25] Jiménez-Sandoval, O., Ramírez-Rosales, D., del Jesús Rosales-Hoz, M., Sosa-Torres, M. E., and Zamorano-Ulloa, R. Magnetostructural behaviour of the complex $[MnL(H_2O)_2]Cl_2\ 4H_2O$ at variable temperature studied by electron spin resonance (L= 2,13-dimethyl-3,6,9,12,18-pentaazabicyclo [12.3.1] octadeca-1(18),2,12,14,16-pentaene). *Journal of the Chemical Society, Dalton Transactions*, (10): 1551-1556, 1998.

[26] Schleife, F., Rodenstein, A., Kirmse, R. and Kersting, B. Seven-coordinate Mn (II) and Co (II) complexes of the pentadentate ligand 2, 6-diacetyl-4-carboxymethyl-pyridine bis (benzoylhydrazone): Synthesis, crystal structure and magnetic properties. *Inorganica Chimica Acta*, 374(1): 521-527, 2011.

[27] Grau, M., Rigodanza, F., White, A. J., Sorarù, A., Carraro, M., Bonchio, M., and Britovsek, G. J. Ligand tuning of single-site manganese-based catalytic antioxidants with dual superoxide dismutase and catalase activity. *Chemical Communications*, 50(35): 4607-4609, 2014 and references therein.

[28] Liu, G. F., Filipovic, M., Heinemann, F. W., and Ivanovic-Burmazovic, I. Seven-coordinate iron and manganese complexes with acyclic and rigid

pentadentate chelates and their superoxide dismutase activity. *Inorganic Chemistry*, 46(21): 8825-8835, 2007.

[29] Lorenzini, C., Pelizzi, C., Pelizzi, G., & Predieri, G. Investigation into aroylhydrazones as chelating agents. Part 3. Synthesis and spectroscopic characterization of complexes of Mn^{II}, Co^{II}, Ni^{II}, Cu^{II}, and Zn^{II} with 2,6-diacetylpyridine bis (benzoylhydrazone) and X-ray structure of aquachloro[2,6-diacetylpyridine bis (benzoylhydrazone)] manganese(II) chloride. *Journal of the Chemical Society, Dalton Transactions*, (4): 721-727, 1983.

[30] Liu, J., Chen, Y. C., Jia, J. H., Liu, J. L., Vieru, V., Ungur, L., and Chen, X. M. A Stable Pentagonal-Bipyramidal Dy (III) Single-Ion Magnet with a Record Magnetization Reversal Barrier over 1000 K. *Journal of the American Chemical Society*, 138(16): 5441-5450, 2016 and references therein.

[31] Giordano, T. J., Palenik, G. J., Palenik, R. C., and Sullivan, D. A. Pentagonal-bipyramidal complexes. Synthesis and characterization of aqua (nitrato)[2, 6-diacetylpyridine bis (benzoyl hydrazone)] cobalt (II) nitrate and diaqua [2, 6-diacetylpyridine bis (benzoyl hydrazone)] nickel (II) nitrate dihydrate. *Inorganic Chemistry*, 18(9): 2445-2450, 1979.

[32] Lorenzini, C., Pelizzi, C., Pelizzi, G., and Predieri, G. Investigation into aroylhydrazones as chelating agents. Part 3. Synthesis and spectroscopic characterization of complexes of Mn^{II}, Co^{II}, Ni^{II}, Cu^{II}, and Zn^{II} with 2,6-diacetylpyridine bis (benzoylhydrazone) and X-ray structure of aquachloro [2,6-diacetylpyridine bis (benzoylhydrazone)] manganese(II) chloride. *Journal of the Chemical Society, Dalton Transactions*, (4): 721-727, 1983.

[33] Bhirud, R. G., and Srivastava, T. S. Synthesis, characterization and superoxide dismutase activity of some ternary copper (II) dipeptide-2, 2′-bipyridine, 1,10-phenanthroline and 2,9-dimethyl-1,10-phenanthroline complexes. *Inorganica Chimica Acta*, 179(1): 125-131, 1991.

[34] Bhirud, R. G., and Srivastava, T. S. Superoxide dismutase activity of $Cu(II)_2(aspirinate)_4$ and its adducts with nitrogen and oxygen donors. *Inorganica Chimica Acta*, 173(1): 121-125, 1990.

[35] Sheldrick, G. M. A short history of SHELX. *Acta Crystallographica Section A: Foundations of Crystallography*, 64(1): 112-122, 2008.

[36] Llunell, M., Casanova, D., Cirera, J., Bofill, J. M., Alemany, P., Alvarez, S., Pinsky, M. and Avnir, D. *SHAPE: Continuous shape measures of polygonal and polyhedral molecular fragments*; University of Barcelona: Barcelona, 2005.

[37] Neese, F. *ORCA - an ab initio, Density Functional and Semiempirical Program Package*; University of Bonn, Germany, 2007.

[38] Becke, A. D. Density-functional exchange-energy approximation with correct asymptotic behavior. *Physical Review A*, 38(6): 3098-3100, 1988.

[39] Perdew, J. P. Density-functional approximation for the correlation energy of the inhomogeneous electron gas. *Physical Review B*, 33(12): 8822-8824, 1986.

[40] Schäfer, A., Huber, C., and Ahlrichs, R. Fully optimized contracted Gaussian basis sets of triple zeta valence quality for atoms Li to Kr. *The Journal of Chemical Physics*, 100(8): 5829-5835., 1994.

[41] Heß, B. A., Marian, C. M., Wahlgren, U., and Gropen, O. A mean-field spin-orbit method applicable to correlated wavefunctions. *Chemical Physics Letters*, 251(5): 365-371, 1996.

[42] Neese, F. Calculation of the zero-field splitting tensor on the basis of hybrid density functional and Hartree-Fock theory. *The Journal of Chemical Physics*, 127(16): 164112-116112, 2007.

[43] Stevens, K. W. H. Matrix elements and operator equivalents connected with the magnetic properties of rare earth ions. *Proceedings of the Physical Society. Section A*, 65(3): 209, 1952.

[44] Wriedt, M., and Näther, C. In situ solid state formation of copper (I) coordination polymers by thermal reduction of copper (II) precursor compounds: structure and reactivity of $[Cu(NCS)_2(pyrimidine)_2]_n$. *Dalton Transactions*, (46): 10192-10198, 2009.

[45] Mautner, F. A., Louka, F. R., LeGuet, T., and Massoud, S. S. Pseudohalide copper (II) complexes derived from polypyridyl ligands: Synthesis and characterization. *Journal of Molecular Structure*, 919(1): 196-203, 2009.

[46] Carranza, J., Sletten, J., Lloret, F., and Julve, M. Preparation, crystal structures and magnetic properties of three thiocyanato-bridged copper (II) complexes with 2,2′-biimidazole or 2-(2′-pyridyl) imidazole as terminal ligands. *Polyhedron*, 28(11): 2249-2257, 2009.

[47] Jiang, G., Bai, J., Xing, H., Li, Y., and You, X. A Tetrahedral Water Tetramer in a Zeolite-like Metal-Organic Framework Constructed from $\{(H_3O)_2[Fe_6O\{(OCH_2)_3CCH_3\}_4Cl_6]\odot 4H_2O\}$. *Crystal Growth & Design*, 6(6) 1264-1266, 2006.

[48] Long, L. S., Wu, Y. R., Huang, R. B., and Zheng, L. S. A Well-Resolved uudd Cyclic Water Tetramer in the Crystal Host of [Cu(adipate)(4, 4-bipyridine)]$\odot(H_2O)_2$. *Inorganic Chemistry*, 43(13): 3798-3800, 2004.

[49] Zuhayra, M., Kampen, W. U., Henze, E., Soti, Z., Zsolnai, L., Huttner, G., and Oberdorfer, F. A Planar Water Tetramer with Tetrahedrally Coordinated Water Embedded in a Hydrogen Bonding Network of $[Tc_4(CO)_{12}\text{-}(\mu_3\text{-}OH)_4\odot 4H_2O]$. *Journal of the American Chemical Society*, 128(2): 424-425, 2006.

[50] Chen, W. J., Long, L. S., Huang, R. B., and Zheng, L. S. A Dihalide–Decahydrate Cluster of $[X_2(H_2O)_{10}]^{2-}$ in a Supramolecular Architecture of $\{[Na_2(H_2O)_6(H_2O@TMEQ[6])]_2(C_6H_5NO_3)\}X_2(H_2O)_{10}$ (TMEQ[6]= α,α′,δ,δ′-Tetramethylcucurbit[6]uril; X= Cl, Br). *Crystal Growth & Design*, 13(6): 2507-2513, 2013.

[51] Ghosh, S. K., Ribas, J., and Bharadwaj, P. K. Metal–organic framework structures of Cu(II) with pyridine-2,6-dicarboxylate and different spacers: identification of a metal bound acyclic water tetramer. *CrystEngComm*, 6(45): 250-256, 2004.

[52] Zein, S., Duboc, C., Lubitz, W., and Neese, F. A systematic density functional study of the zero-field splitting in Mn(II) coordination compounds. *Inorganic Chemistry*, 47(1): 134-142, 2008.

[53] Liu, G.F., Filipović, M., Heinemann, F.W. and Ivanović-Burmazović, I. Seven-coordinate iron and manganese complexes with acyclic and rigid pentadentate chelates and their superoxide dismutase activity. *Inorganic Chemistry*, 46(21): 8825-8835, 2007.